Air Void Characterization in Fresh Cement Paste through Ultrasonic Attenuation using an Immersion Procedure

A Thesis
Presented to
The Academic Faculty

by

Natalie Darraugh

In Partial Fulfillment
of the Requirements for the Degree
Masters of Science in the
School of Civil and Environmental Engineering

Georgia Institute of Technology
December 2009

Air Void Characterization in Fresh Cement Paste through Ultrasonic Attenuation using an Immersion Procedure

Approved by:

Dr. Laurence J. Jacobs, Advisor
School of Civil and Environmental Engineering
Georgia Institute of Technology

Dr. Kimberly Kurtis, Co-Advisor
School of Civil and Environmental Engineering
Georgia Institute of Technology

Dr. Jin-Yeon Kim
School of Civil and Environmental Engineering
Georgia Institute of Technology

Date Approved: August 19, 2009

ACKNOWLEDGEMENTS

I must first and foremost thank my reading committee for their immense support both in the classroom and in the lab: Dr. Laurence J. Jacobs, my advisor, Dr. Kimberly Kurtis, my co-advisor, and Dr. Jin-Yeon Kim. It was due to the encouragement and extra nudge of Dr. Jacobs and Dr. Kurtis that I dared to undertake undergraduate and graduate research and a Master's thesis at all. And since it all began over two and a half years ago, they all have provided me with an incredibly amount of knowledge and resources in order to help me succeed.

I wish to recognize the Georgia Department of Transportation for their support of my work. I would also like to thank Terry Vines of Lafarge for providing additional services and saving me an immense amount of time, and Jeremy Mitchell and Andy Udell of Georgia Tech facilities for helping me build not only my current apparatus but all the failed designs that came before it.

To the graduate students who have made my work possible, I owe many thanks. I could not have come this far without the previous work of Wonsiri "Bo" Punurai and Richard Kmack. Many thanks to Amal Jayapalan for technical assistance in the lab. And of course to my lab companions, for many laughs and camaraderie during late nights in the lab.

Finally, I would like to thank my family and friends for their love and support. They may not understand what I'm working on half the time, but somehow they still tell me it's great. They've been with me from the beginning and will have to deal with me until the end, and for that I am incredibly thankful.

TABLE OF CONTENTS

LIST OF TABLES

LIST OF FIGURES

SUMMARY

The most prevalent method for the prevention of freeze-thaw and salt scaling damage in cement based materials is through the entrainment of air voids using air entraining chemical admixtures (AEA's). However, the common field methods for measuring air content in fresh concrete cannot distinguish between entrained and entrapped air voids, and the actual air content in the hardened concrete can vary from that determined by these tests due to a variety of factors such as workability, placing operations, consolidation efforts, and environmental conditions. Previous research has shown the ability of ultrasonic attenuation to distinguish between entrained and entrapped air voids in hardened cement paste, providing a foundation for an inversion procedure to calculate the size and volume content of the two scatterer sizes. While additional challenges are present with measurements in fresh paste, the use of an immersion setup can overcome the limitations of cement paste containment vessels and provide a means to measure air content from batching to placement. An immersion apparatus to monitor ultrasonic wave attributes including attenuation in fresh cement paste is designed and built. Results comparing air entrained and non-air entrained cement pastes are presented. Ultrasonic wave attributes are studied as a function of time and level of chemical air entrainer. Finally, recommendations are made to improve the accuracy of the immersion apparatus in order to develop an in situ, quality control procedure to quantify the air content of fresh cement paste from batching to placement.

CHAPTER 1

INTRODUCTION

Freezing and thawing cycles cause damage to concrete structures in the form of scaling, spalling, and map cracking, which negatively affects their structural integrity and impermeability. This damage phenomenon is a widespread issue affecting most of the continental United States. In the construction industry, chemical air entraining admixtures (AEA's) are commonly used in concrete mixes to help mitigate this damage. AEA's set up a stable network of entrained air voids in concrete to accommodate the expansive freezing water. These entrained air voids are generally 0.01-1 mm. in size and ideally provide a regularly spaced system of voids. However, a second type of void exists in cement-based materials called entrapped air, and these larger voids are undesirable as they are detrimental to the overall strength and impermeability of the structure.

While it is important to have an adequate system of entrained air voids to prevent freeze-thaw damage, the current standardized test methods available to evaluate the air void system in fresh concrete [1-3] are limited. These tests cannot measure air content in situ, and they neglect the effects of delivery, placement, consolidation, and environmental exposure. Furthermore, these tests cannot distinguish between desirable entrained air voids and larger, irregular entrapped voids. Therefore, it would be desirable to have a field test that could differentiate between these two types of voids and that could be used to measure air content from batching to placement.

Previous work has been completed by Punurai et al [4-6] using ultrasonic attenuation to determine air content in hardened cement paste specimens. Because hardened cement paste is rigid, static, and less absorptive, acoustic modeling and ultrasonic measurements are less problematic for this material than for plastic cement paste. Punarai was able to relate ultrasonic attenuation to air content in hardened cement pastes, and developed an inversion method to iteratively solve for the volume fraction and radius of air voids in the sample. This research measured an increase in attenuation with increasing levels of air content. It was also observed that the entrained air volume fraction dominated the higher frequency response, while the larger entrapped voids dominated the lower frequency response. While this work showed the ability of ultrasonic attenuation to measure air content and differentiate between entrained and entrapped voids, these results in hardened paste are not applicable for real-time quality control. They are only valid for characterization of the material after final setting, at which point it is too late to make any mix adjustments. Ideal quality control testing occurs on site and only requires minutes to hours, so that any issues can be immediately addressed. Thus in order to develop a realistic quality control test for cement based materials using ultrasonic testing, fresh cement paste must be considered.

Because fresh cement-based materials behave like a viscous fluid, much consideration has been given to the containment of the material in order to best measure ultrasonic attributes. The most commonly used experimental setup confines the paste between acrylic sheets and fixes the transducers outside the containment vessel as proposed by [7]. While only a small portion of previous research on ultrasonic characterization of fresh

cement-based materials has studied air content, there has been a considerable amount of work on monitoring setting time and strength gain [7-10]. For example, Sayers and Dahlin [8] examined the development of ultrasonic waveforms as a function of time in American Petroleum Institute class G cement pastes for the purpose of studying strength gain. Using an acrylic containment vessel and externally mounted transducers, they examined ultrasonic signals in both the time and frequency domains over the first 25 hours of hydration. In one design mix, they observed two wave components—one higher frequency and one lower frequency wave—in the ultrasonic signals during the first few hours of hydration. They proposed that as the cement paste hydrates and begins forming an interconnected solid phase, this behavior can be modeled using Biot's theory for wave propagation in fluid-saturated porous media.

Kmack [11] applied Punarai's work to fresh paste samples in an effort to develop an ultrasonic test to measure air content in plastic cement-based material. However, because fresh cement paste is inherently more attenuative than hardened cement paste, inadequate signal strength became a serious concern. As will be further discussed in Chapter 4, Kmack was limited by the measurement apparatus, specifically the cement paste containment vessel, and was unable to calculate absolute values of ultrasonic attenuation. Still, he was able to monitor signal strength and pulse velocity of fresh cement paste samples over the first 12 hours of hydration, and did correlate a decrease in signal strength and pulse velocity with increasing levels of AEA.

The lack of an effective, in situ test method for measuring air content in plastic concrete and the limited amount of research on ultrasonic wave propagation in fresh cement-based materials provided the motivation for this work. The objective of this research is to monitor ultrasonic wave attributes including attenuation in fresh cement paste as a function of hydration time and level of chemical air entrainer, and to establish an in situ, quality control procedure to quantify the air content of fresh cement paste from batching to placement.

CHAPTER 2

CEMENT-BASED MATERIALS

2.1 Portland cement

2.1.1 Cement components

The four main mineral phases of Portland cement are dicalcium silicate (C_2S), tricalcium silicate (C_3S), tricalcium aluminate (C_3A), and tetracalcium aluminoferrite (C_4AF). These compounds are the most significant in determining the characteristics of cement-based materials both during hydration and after final set. Varying the levels of each of these components can affect the reaction rate, heat evolved, setting time, void space, density, rate of strength gain, ultimate strength, dimensional stability, and durability of the material. Other typical Portland cement components can include gypsum, magnesium oxides, calcium oxide (free lime), and alkalis. While these components do contribute to the properties of cement-based materials, they are typically present in smaller fractions. Gypsum, for example, is added at rates of 5-7% by mass to slow the rapid reaction of the C_3A phase and prevent "flash set" of the mix.

C_3S ($3CaO \cdot SiO_2$): C_3S generally makes up 45-60% of a Portland cement. It reacts rapidly, providing strength and contributing to stiffening as early as 2-3 hours after mixing and continuing through the first 7 to 14 days. Because of its

rapid strength gain, the time of initial set of a cement paste is directly related to the level of C_3S present in the cement clinker. The hydration reaction of C_3S also generates a moderate amount of heat, about twice that of C_2S. Because it forms the largest component in Portland cement, it contributes more heat than any other phase to the total heat evolution of the hydrating cement paste.

C_2S ($2CaO \cdot SiO_2$): The level of C_2S in a Portland cement is between 15-30%. It hydrates and stiffens at a much slower rate than C_3S and does not significantly contribute to the strength of the hydrated cement paste until about seven days. Unlike C_3S, the hydration reaction between C_2S and water evolves a relatively low level of heat. Because of its slower reaction rate and the fact that the hydration of C_2S produces less calcium hydroxide, or CH, than that of C_3S, a higher ratio of C_2S to C_3S produces a denser microstructure.

C_3A ($3CaO \cdot Al_2O_3$): C_3A typically contributes 6-12% to the total compound composition of a Portland cement. As mentioned above, the ordinarily very rapid reaction of this phase is controlled by the addition of gypsum to the ground cement clinker. Even in the presence of gypsum, it reacts relatively rapidly and its hydration products contribute to early stiffening of cement-based matrices. However, its contribution to strength development is small. Additionally, the hydration of C_3A liberates a very large level of heat, making its contribution to total heat evolution typically the second most significant, given its generally relatively small fraction in Portland cement.

C_4AF ($4CaO \cdot Al_2O_3 \cdot Fe_2O_3$): Ordinarily responsible for 6-8% of the total composition of a Portland cement, C_4AF contributes very little to the strength

development of a hydrating cement paste. It also only contributes a moderate level of heat even though it hydrates rapidly. Its primary function is to reduce the clinkering temperature and therefore the level of energy required in the production of Portland cement.

2.2 Hydration of Portland cement

Upon mixing Portland cement with water, the various components in cement chemically react with water during the first 24 hours to transform the mixture into a solid, cohesive hydrated cement paste. These reactions can occur through solution by which the cement components dissolve and form hydrates in solution before precipitating, or they can occur as topochemical reactions on or very near the surface of the reacting cement grains. As hydration proceeds, capillary porosity and permeability decrease while strength, stiffness, and total heat evolution increase. The rate at which this occurs not only depends on the cement composition, but also the cement fineness and the water-to-cement ratio (w/c), as well as environmental conditions (e.g., temperature, availability of moisture). The addition of different chemical admixtures can affect the hydration kinetics as well. Figure 2.1 from Mehta and Monteiro [12] illustrates the scale of the major components of a hydrated cement paste. A summary of these various components follows.

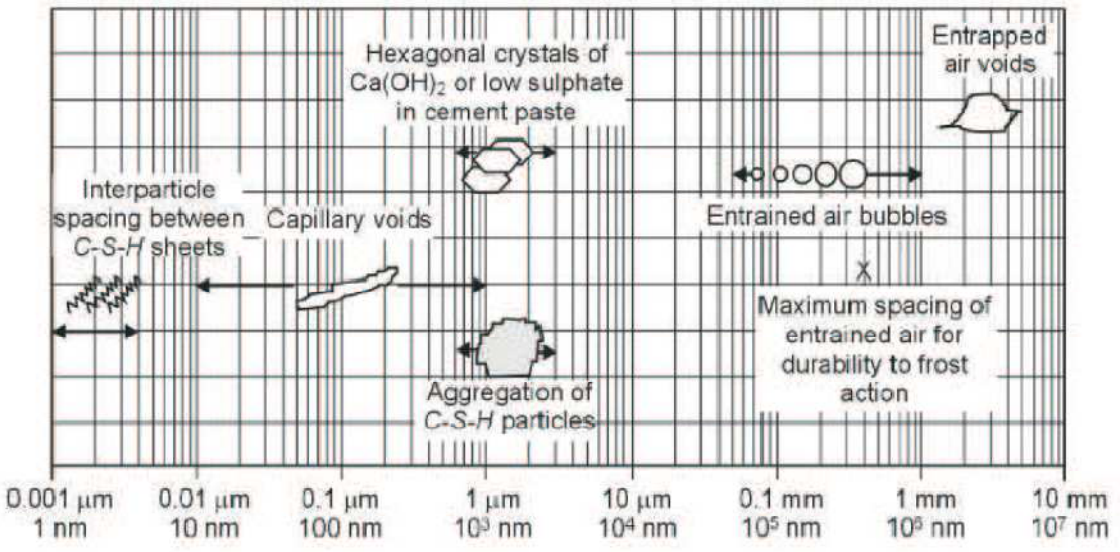

Figure 2.1: Dimensional scale of solids and voids in hydrated cement paste [12]

2.2.1 Solid hydration products

There are four principal solid phases present in hydrated cement paste: calcium silicate hydrate (C-S-H), calcium hydroxide (CH), calcium sulfoaluminates, and unhydrated clinker grains. Figure 2.2 from [13] shows the relative amount of the each hydration product as a function of time. Ettringite—a needle-shaped calcium sulfoaluminate—and calcium hydroxide—a crystal with morphologies ranging from platey to irregular—are among the first compounds formed, appearing within minutes of initial mixing. Calcium silicate hydrate begins to form a few hours later on the surfaces of the hydrating cement grains, and ultimately in the space previously occupied by the cement grains. A second calcium sulfoaluminate, monosulfate hydrate, can form after a few days upon the decomposition of ettringite, as the availability of sulfate ions grows limited. The presence of residual unhydrated clinker grains is a function of the particle size

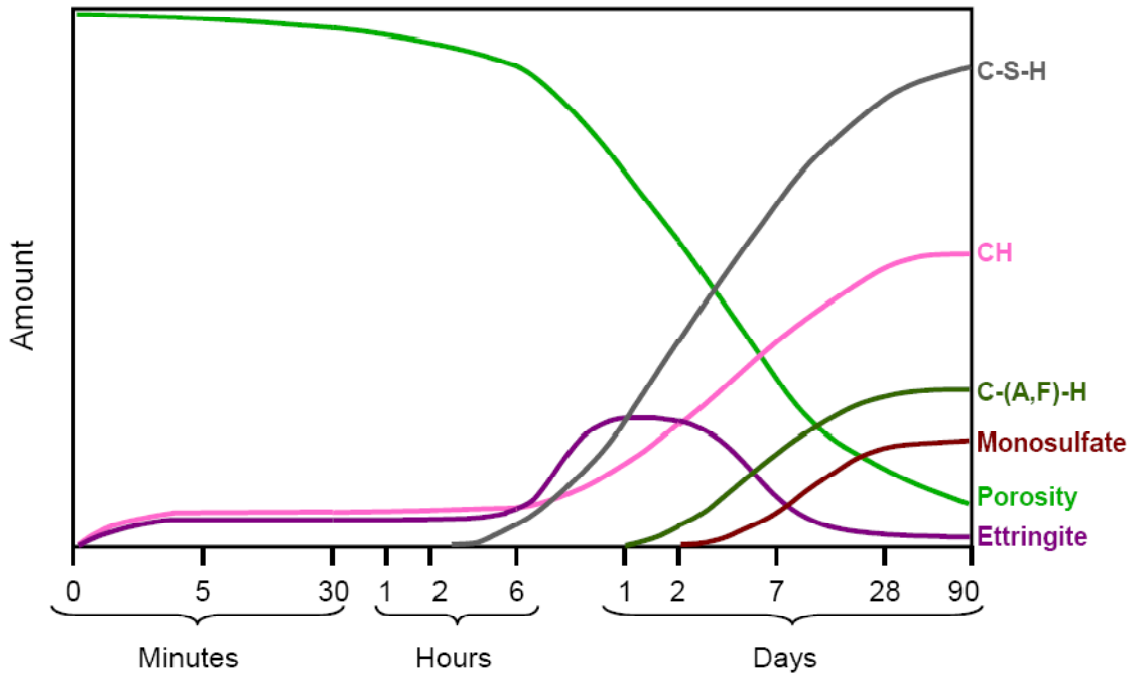

Figure 2.2: Formation of various hydration products with time [13]

distribution of the cement and the degree of hydration. Each of the four main reaction products contributes to different properties to the hydrated cement paste.

Calcium silicate hydrate (C-S-H): C-S-H constitutes between 50-60% of the solid volume of the hydrated cement paste. While the compound itself is not well understood and its composition varies, the ratio of calcium to silica is typically between 1.1 and 2. The overall structure consists of layers of calcium and silica with water bound both chemically and physically to the structure. Due to its very high surface area, numerous ionic and covalent bonds as well as secondary hydrogen and van der Waals bonds exist between the C-S layers. Drawing from

the high level of bonding within the complex structure, it is the primary strength-giving phase in hydrated Portland cement paste.

Calcium hydroxide (CH): Calcium hydroxide typically accounts for 20-25% of the total volume of solids. Unlike C-S-H, the composition of calcium hydroxide is fixed and can be described stoichiometrically as $Ca(OH)_2$. Its crystals generally develop a hexagonal-prism structure, however, its morphology can vary slightly based on available space, temperature of hydration, and existing impurities. Because its considerably lower surface area decreases the potential for van der Waals forces, calcium hydroxide does not contribute significantly to the overall strength of the hydrated cement paste. Additionally, calcium hydroxide is more soluble than C-S-H, making a hydrated cement paste with higher levels of calcium hydroxide more susceptible to attack by acidic and sulfate-containing solutions.

Calcium sulfoaluminates: Calcium sulfoaluminates, which include ettringite, monosulfate hydrate, calcium aluminate hydrates, and ferric-aluminum hydroxide gels, occupy 15-20% of the solid volume of hydrated cement paste. During early hydration, ettringite formation aids in the stiffening of the cement paste and provides a minor contribution to early strength. However in the days after hydration, ettringite can become unstable and decompose into monosulfate hydrate, which forms as hexagonal-plate crystals. Because the presence of monosulfate hydrate increases the vulnerability of a cement paste to sulfate attack, ettringite is the more favorable calcium sulfoaluminate for durability considerations.

Unhydrated clinker grains: As hydration proceeds, the level of unhydrated clinker grains decreases due to the dissolution of the cement particles into solution and the subsequent chemical reaction. However in nearly all hydrated cement pastes, anhydrous cement will remain. The level of unhydrated clinker grains remaining in a hydrated cement paste decreases with time. It can also be minimized by decreasing the particle size distribution, typically through finer grinding of the cement clinker, and increasing the degree of hydration which can be achieved through the use of a higher w/c and by providing adequate, moist curing conditions.

2.2.2 Voids

Voids in a hydrated cement paste can range in size from less than a nanometer up to a few millimeters. Depending on the size and type, these voids influence the properties of the cement paste in different but significant ways. The four void types are discussed below.

Interlayer space in C-S-H: The interlayer space within the C-S-H structure ranges from 0.5-2.5 nm in width, providing for 28% porosity in solid C-S-H [12]. Water is often bound along the void surfaces through hydrogen bonding, however, the properties of the C-S-H interlayer space are thought to be independent of the w/c. Due to their size, these voids are too small to negatively affect the strength or permeability of the hydrated cement paste.

Capillary Voids: The irregularly shaped capillary voids represent the volume in the hydrated cement paste not occupied by either solid hydration products or anhydrous cement grains. Due to their origin, the volume and size of the capillary voids are a function of the w/c and the degree of hydration. While a well hydrated cement paste with a low w/c will typically have capillary voids that range from 2.5-50 nm in size, these voids can be up to 5 μm in size in a high w/c cement paste at early ages. Due to the large range in size, two classifications of capillary voids exist, each contributing to slightly different characteristics of the hydrated cement paste. Macropores are considered to be those larger than 50 nm in size and adversely affect the strength and permeability of the cement paste. Capillary voids less than 50 nm are classified as micropores, and they influence the drying shrinkage and creep.

Entrained Air Voids: Entrained air voids can range from 10 μm up to 1 mm in size and are generally spherical in shape. They are typically introduced through the use of chemical surfactants called air entraining admixtures (AEA's) that cause the water to bubble upon mixing with cement, thereby setting up a stable system of voids. Figure 2.3 shows a digital image of two hardened cement paste samples both with a water to cement ratio (w/c) of 0.35, but the bottom specimen contains 0.4% chemical air entrainer by mass of cement. Because these voids are relatively small and disconnected, they do not adversely affect the permeability and porosity of the mix. They can, however, cause some decrease in strength—a 1% increase in entrained air can cause about a 5% decrease in strength [5]. Chemical air entrainers reduce segregation and bleeding and increase workability,

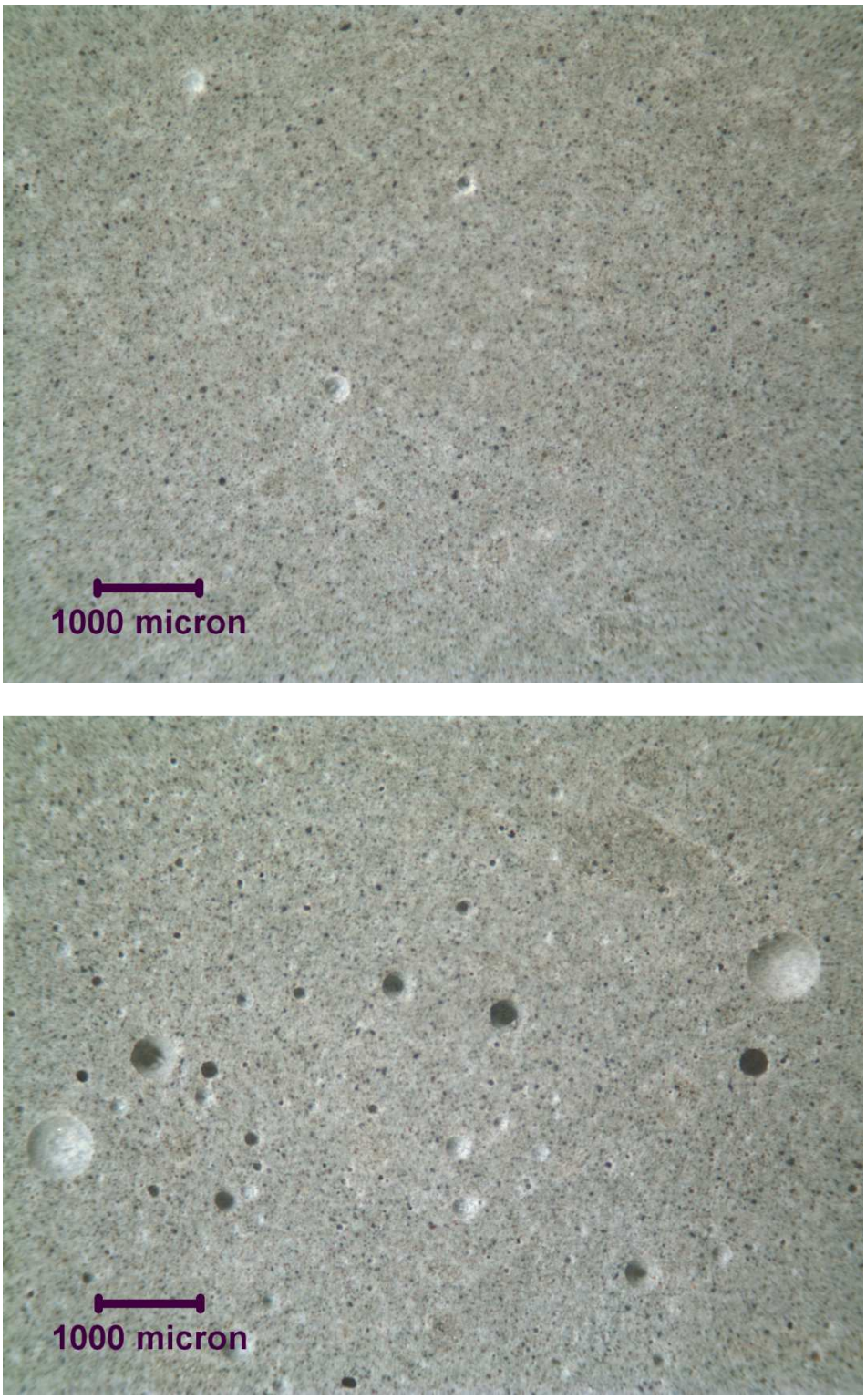

Figure 2.3: Hardened cement pastes with 0% (top) and 0.4% (bottom) AEA

though, acting as a water reducer. Therefore, an equivalent slump and workability can be achieved with a lower w/c when AEA's are used, which counteracts the slight decrease in strength due to the entrained air voids.

Entrapped Air Voids: Entrapped air voids are generally larger than 1 mm in size. They are irregular in spacing and shape and are too large and disconnected to provide any freeze-thaw resistance. They also cause a decrease in strength, but unlike entrained air voids, they cause an increase in permeability and porosity, making a mix more susceptible to the ingress of various salts, ions, and water. Entrapped air voids are most often introduced into a mix through the various mixing procedures but can also result from poor consolidation. Additionally, mix designs with lower workability are more disposed to the formation of entrapped air voids. Proper compaction methods, such as rodding or vibration, should be used be reduce the level of entrapped air. However, 1-2% of entrapped air is usually present in hardened cement-based materials.

2.3 Freeze-thaw action

Saturated or near-saturated cement based materials subject to freezing and thawing cycles are susceptible to damage. In the cement matrix, this damage usually manifests in the form of scaling, spalling, map cracking, and/or D-cracking. Figure 2.4 shows some images from PCA of typical freeze-thaw damage [14]. As shown in Figure 2.5, freeze-thaw damage affects much of the continental U.S [15]. While the exact mechanisms

Figure 2.4: Images showing spalling (top) and popout (bottom) due to free-thaw [14]

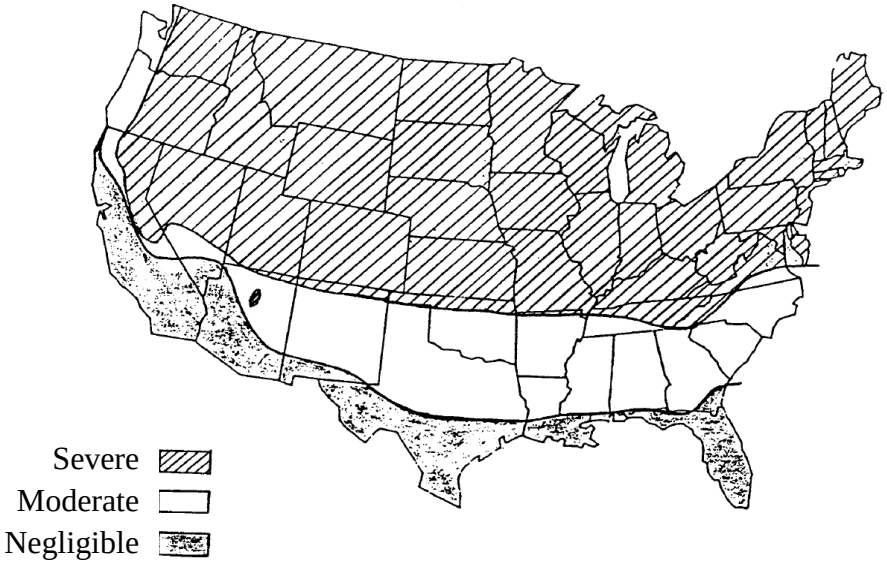

Figure 2.5: Locations and severity of freeze-thaw damage [15]

behind freeze-thaw damage are not entirely understood, it is believed that freezing water in the matrix causes a buildup of hydraulic pressure, osmotic pressure, or some combination of the two. The expansion of the freezing water compresses the remaining pore solution, and the pressure can only be alleviated if the remaining water escapes to empty space within or beyond the surface of the material. However, the cement paste matrix resists the movement of the water, leading to undesirable expansion of the water as it freezes in the matrix, increasing hydraulic pressure, and possibly cracking in the matrix. Additionally due to the freezing of water out of the pore solution, a more concentrated solution of ions is created locally. This sets up a concentration gradient that causes the water to flow towards the freezing sites leading again to increased osmotic pressure and possibly cracking.

The most prevalent method for the prevention of freeze-thaw damage is through the entrainment of air voids within the cement paste, most often by the use of air entraining chemical admixtures (AEA's). In cement-based materials, soluble salts (usually sodium) of wood resins, wood rosins, lignosulfonic acid, sulfonated hydrocarbons and fatty acids are among the common chemicals used in air entraining admixtures [16]. The entrainment of air voids can also be achieved through the use of air entraining anhydrous cements, where similar air entraining agents are interground with the cement clinker. AEA's are most often surfactants with a hydrophilic polar group attached to a non-polar hydrocarbon chain. While the hydrophilic head can be anionic, cationic, nonionic, or amphoteric, most modern AEA's are anionic due to the increased stability of their resulting air void systems [17]. As such, the following discussion will assume the

hydrophilic head to be anionic. In aqueous solutions, the polar groups orient towards the water thereby lowering the surface tension and promoting bubble formation as the hydrophobic hydrocarbon chain becomes oriented into the air bubbles. Additionally, the negatively charged ions that form on the surface of the air bubbles act as a barrier preventing the coalescence of bubbles as illustrated in Figure 2.5 [18]. This surface

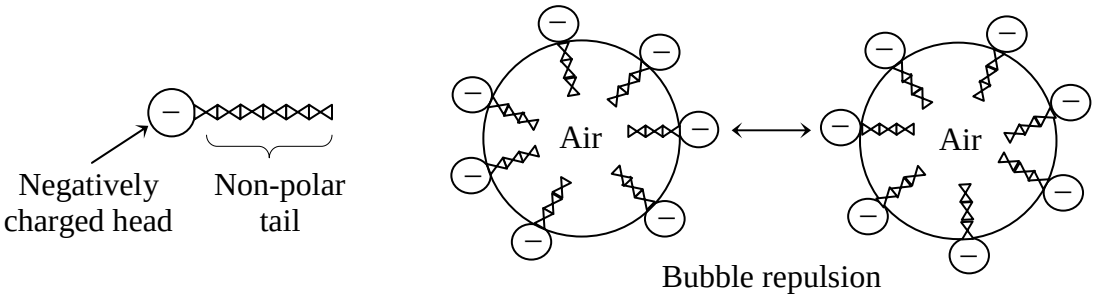

Figure 2.5: Anionic air entraining molecule and its orientation at the bubble interface [18]

charge also causes secondary bonding between the air bubbles and positively charged locations on both the cement grains and aggregate particles forming chains of alternating air bubbles and cement or aggregate particles. The weakly bonded chains improve cohesion, but also allow shear displacement between chains thereby increasing workability.

The entrained air voids provide a regularly spaced but disconnected network of air voids to accommodate the expanding, migrating water. Still, the volume of entrained air is dependent upon many factors other than dosage of chemical air entrainer. In general, air content increases with increasing cement alkali content, sand content, and sand coarseness, and decreasing cement content and fineness, temperature, and workability

[18]. However the factors affecting air content are truly much more complicated. The effectiveness of the AEA is related to both its ability to promote bubble formation and also stabilize the air void system. For example, the use of crushed rocks versus river gravels as aggregate produces higher stresses during the mixing procedure, resulting in lower air content [17]. Additionally, an increase in slump will increase air content up to a certain point, but beyond which continued increase actually decreases total air volume. Therefore a given level of AEA will not produce identical air volume fractions or distributions between different mixes. While the volume of air required to prevent freeze-thaw damage varies based on the exposure conditions and the mix specifications, ACI generally recommends between 3-8% entrained air by volume as shown in Table 2.1 [19]. To provide better freeze-thaw resistance, the spacing factor for the entrained air voids should ideally be less than 0.2 mm to decrease the travel distance of the migrating water [4].

2.4 Air void characterization methods

Currently, test methods exist to measure air content in both fresh and hardened concrete. ASTM C457 [20] provides two methods to quantify air content in hardened concrete by petrographic analysis. While petrographic results tend to be more accurate than those provided by fresh concrete tests, their results are not immediately available because they require the use of hardened samples which must be cut and polished prior to analysis. Some of the common field methods for quantifying the total air content in fresh concrete

Table 2.1: Air contents for frost-resistant concrete as recommended by ACI [19]

Nominal maximum aggregate size, in (mm)	Average air content, (%)[a]	
	Severe explosure[b]	Moderate exposure[c]
3/8 (9.5)	7-1/2	6
1/2 (12.5)	7	5-1/2
3/4 (19.0)	6	5
1 (25)	6	5
1-1/2 (37.5)	5-1/2 [d]	6 [d]
3 (75)	4-1/2 [d]	3-1/2 [d]
6 (150)	4	3

[a] A reasonable tolerance for air content in field construction is $\pm 1 - 1/2\ \%$

[b] Outdoor exposure in a cold climate where the concrete maybe in almost continuous contact with moisture before freezing or where deicing salts are used. Examples are pavements, bridge decks, sidewalks and water tanks.

[c] Outdoor exposure in a cold climate where the concrete will be on ly occasionally exposed to moisture before freezing and where no deicing salts will be used. Examples are certain exterior walls, beams, girders, and slabs not in direct contact with soil.

[d] These air contents apply to the whole as for the preceding aggregate sizes. When testing these concretes, however, aggregate larger than 1-1/2 in. (37.5 mm) is removed by handpicking or sieving and the air content is determined on the minus 1-1/2 in. (37.5 mm) fraction of the mixture. (The field tolerance applies to this value.) From this, air content of the whole mixture is computed.

Note: There is conflicting opinion on whether air contents lower than those given in the table should be permitted for high-strength (approximately 5500 psi (37.8 MPa)) concrete. The committee believes that where supporting experience practices and exposure, the air contents can be reduced by approximately 1%. (For nominal maximum aggregate sizes over 1-1/2 in. (37.5 mm), this reduction applies to the minus 1-1/2 in. (37.5 mm) fraction of the mixture.

include the Pressure Method (ASTM C 231) [1], the Volumetric Method (ASTM C 173) [2], and the Gravimetric Method (ASTM C 138) [3]. However according to [1, 2] the actual air content in the hardened concrete can vary from that determined by these tests due to a variety of factors such as consolidation, uniformity and stability of the bubbles, time of comparison, environmental exposure, and stage in delivery. Additionally, the pressure method cannot be used for mixes containing lightweight aggregates. Therefore, these test methods do not account for the effects of placing and compacting or other factors on site (e.g., changes in temperature) which may affect the quality of the air entrainment. As such, tests done on samples of limited size which are placed and compacted in a standardized way, may not be representative of the in situ material. Further, these standard methods provide a measure of total air content and cannot distinguish between desirable entrained and undesirable entrapped air.

Recently, a new system has been developed to determine the air volume and size distribution of voids in fresh mortar. The apparatus, called the air void analyzer, uses Stokes' law to determine bubble size based on the rate by which the voids rise through a column of fluid. The larger bubbles ascend faster, and as the voids collect at the top of the cylinder, their buoyant force is measured as a function time. However, in order to test the material, a wire cage is vibrated into the fresh concrete, which allows only the sampling of mortar, excluding aggregate larger than 6 mm. Then, the material is typically transported offsite, and a syringe is used to extract 20 cm^3 of the sample and inject it into the cylinder. However, extracting the sample and transferring it from the site cause further disturbances to the sample, and the assumption that the air content and

size distribution of the sample are representative of that for the in-place concrete must be called into question. Due to its small sample size and variation in sample handling from that of the in-place structure, the practicality and accuracy of this method as a field test are debatable. At the present time, no standard exists for testing with the air void analyzer.

This research will introduce an immersion apparatus that could be used to monitor the air content in plastic cement-based materials from batching to placement and could potentially distinguish between entrained and entrapped air.

CHAPTER 3

ULTRASONIC WAVE PROPAGATION

3.1 Three-dimensional wave propagation

For any closed region of a body subject to body forces, f_i, with displacements, u_i, and principal stresses, σ_{ij}, based on the balance of linear momentum, the stress equations of motion can be written as [22]

$$\sigma_{ij,j} + \rho f_i = \rho \ddot{u}_i. \tag{3.1}$$

In order remove the stresses from Eq. (3.1) and describe the equations of motion in terms of displacement alone, Hooke's law may be applied along with a statement of compatibility between strain and displacement. In general form for any homogeneous material, Hooke's law is given by

$$\sigma_{ij} = C_{ijkl}\epsilon_{kl}. \tag{3.2}$$

For an isotropic material,

$$C_{ijkl} = \lambda\delta_{ij}\delta_{kl} + \mu(\delta_{ik}\delta_{jl} + \delta_{il}\delta_{jk}) \tag{3.3}$$

where μ and λ are the Lamé constants and $\delta_{ij} = \begin{cases} 1 \; if \; i = j \\ 0 \; if \; i \neq j \end{cases}$. Substituting Eq. (3.3) into Eq. (3.2), Hooke's law for isotropic materials simplifies to

$$\sigma_{ij} = \lambda\delta_{ij}\epsilon_{kk} + 2\mu\epsilon_{ij}. \tag{3.4}$$

Assuming linear elastic behavior of the material, any component of the strain tensor, $\boldsymbol{\epsilon}$, can be defined as

$$\epsilon_{ij} = \frac{1}{2}(u_{i,j} + u_{j,i}) \tag{3.5}$$

which, upon substituting this definition into Eq. (3.4) and subsequently into Eq. (3.1), leads to Navier's—or the displacement—equations of motion if body forces are neglected

$$(\lambda + \mu)u_{j,ji} + \mu u_{i,jj} = \rho \ddot{u}_i. \tag{3.6}$$

These equations must be satisfied for every point within the closed region of the body.

3.1.1 Plane time harmonic waves

One particular solution to Eq. (3.6) which represents a plane displacement wave propagating in a half space is given by

$$\boldsymbol{u} = f(\boldsymbol{x} \cdot \boldsymbol{p} - ct)\boldsymbol{d} \tag{3.7}$$

where $\boldsymbol{p}$ and $\boldsymbol{d}$ are unit vectors representing the direction of propagation and the direction of particle motion respectively, and c is the phase velocity. Substituting Eq. (3.7) into Eq. (3.6) one obtains

$$(\mu - \rho c^2)\boldsymbol{d} + (\lambda + \mu)(\boldsymbol{p} \cdot \boldsymbol{d})\boldsymbol{p} = 0. \tag{3.8}$$

For all points within the body, $\boldsymbol{x} \cdot \boldsymbol{p}$ is constant and describes the planes of constant phase which are normal to the propagation direction, $\boldsymbol{p}$. In order to satisfy Eq. (3.8), there are two possible solutions: $\boldsymbol{d} = \pm\boldsymbol{p}$ or $\boldsymbol{p} \cdot \boldsymbol{d} = 0$, or in other words, $\boldsymbol{d}$ must be either parallel or perpendicular to $\boldsymbol{p}$.

Case 1: $\boldsymbol{d} = \pm\boldsymbol{p}$ or $\boldsymbol{d}$ is parallel to $\boldsymbol{p}$ leads to $\boldsymbol{p} \cdot \boldsymbol{d} = \pm 1$. For this case, Eq. (3.8) simplifies to $\lambda + 2\mu - \rho c^2 = 0$ or $c = \sqrt{\frac{\lambda+2\mu}{\rho}} = c_L$. This case represents particle

motion parallel to the propagation direction which describes a longitudinal or P-wave.

Case 2: $\boldsymbol{p} \cdot \boldsymbol{d} = 0$ or $\boldsymbol{d}$ is perpendicular to $\boldsymbol{p}$ provides for Eq. (3.8) to simplify to $\mu - \rho c^2 = 0$ or $c = \sqrt{\frac{\mu}{\rho}} = c_T$. This case represents particle motion normal to the propagation direction which describes a transverse or shear wave.

If the propagating wave is further characterized as a time harmonic wave, the function $f(\boldsymbol{x} \cdot \boldsymbol{p} - ct)$, in Eq. (3.7) can be described as an exponential function yielding

$$\boldsymbol{u} = A\boldsymbol{d}e^{ik(\boldsymbol{x}\cdot\boldsymbol{p}-ct)} \tag{3.9}$$

where *A* describes the magnitude of the particle motion, or the wave amplitude, and $k=2\pi/\Lambda$ is the wave number which describes the number of wavelengths, Λ, over 2π. In terms of the circular frequency, ω, $\mathrm{k} = \omega/\mathrm{c}$.

3.1.2 Reflection and mode conversion

Until now, an infinite half-space has been considered. However, upon taking into account a finite media in the direction of propagation and the existence of a boundary between two half-spaces, reflections and coupling must be incorporated. At the interface, four conditions of continuity must be satisfied, two of stress, and two of displacement. In order to satisfy these continuity conditions, two reflected and two refracted waves potentially exist for each incident wave. However, if a wave is incident upon a stress free boundary ($\sigma_{12} = 0$ *and* $\sigma_{22} = 0$) then only the two reflected waves are required. As shown in Figure 3.1, a P-wave or SV-wave incident upon a free surface has the potential to

produce two reflected waves, one being of the same type as the incident wave and the second being of opposite type. This phenomenon by which a single incident wave produces two reflected waves of different types is called mode conversion.

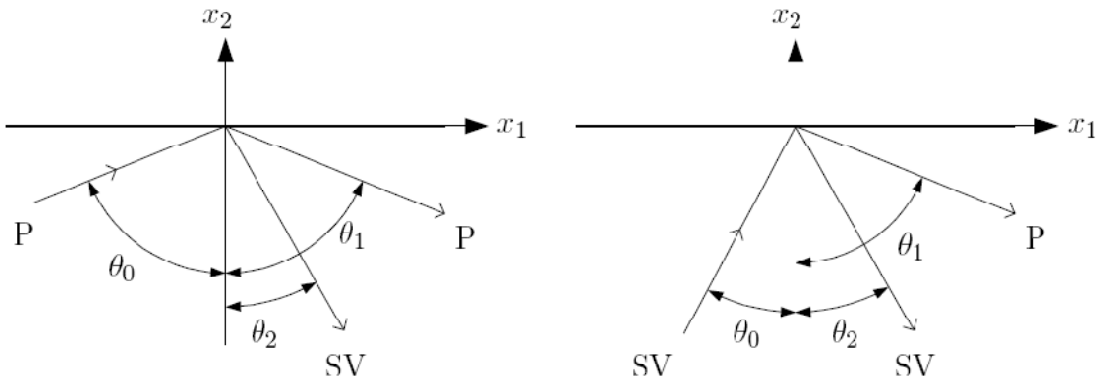

(a) Reflection of a P-wave (b) Reflection of a SV-wave

Figure 3.1: Reflection and mode conversion of incident waves

The incident and reflected harmonic waves traveling in the x_1, x_2-plane can be expressed as:

$$\boldsymbol{u}^{(n)} = A_n \boldsymbol{d}^{(n)} \exp\left\{ik_n\left(x_1 p_1^{(n)} + x_2 p_2^{(n)} - c_n t\right)\right\} \tag{3.10}$$

where the value for the index *n* denotes the various waves, and $n = 0$ corresponds to the incident wave. Note that the angular frequency, $\omega = k_n c_n$ is constant for both the incident and reflected waves. In order to obtain non-trivial amplitudes, A_n, Snell's law must be satisfied, providing a relationship between the angles of incidence, θ_0, θ_1, θ_2, and the wave numbers, k_0, k_1, k_2:

$$k_0 \sin\theta_0 = k_1 \sin\theta_1 = k_2 \sin\theta_2. \tag{3.11}$$

If a P-wave or SH-wave is considered, two unique cases exist in which only one wave is reflected. For $\theta_0 = 0$, or the case of normal incidence, only a single wave of identical

form will be reflected. In other words, a normally incident P-wave will generate only a reflected P-wave. The reflected wave is in phase with the incident wave, and superposition of the two will produce a standing wave. For the second case where $\theta_0 > \theta_{critical}$, the single reflected wave is of opposite form as the incident wave, or more specifically, a P-wave with incident angle greater than $\theta_{critical}$ will produce only a SV-wave. In this case, the waveform that would be reflected of identical type as the incident wave instead generates a Rayleigh surface wave that travels in the x_1 direction and decays exponentially in the x_2 direction.

3.2 Attenuation

Attenuation can be described as the loss in acoustic energy from a propagating sound wave. If a non-attenuative harmonic wave is considered, the stress, σ, can be described as

$$\sigma = \sigma_0 e^{i(kx-\omega t)}. \tag{3.12}$$

For a wave propagating through an attenuative media, a complex wave number, $\tilde{k} = k + i\alpha$, is considered, where α is the attenuation coefficient. In general, α is a function of frequency, ω, but independent of x. Note that here the phase velocity, c, is related only to the real part of $\tilde{k}$, and the equation $k = \omega/c$ is still valid. Substituting in the complex description of the wave number, $\tilde{k}$, it can be seen that the pressure amplitude of the wave decreases exponentially with x:

$$\sigma = \sigma_0 e^{-\alpha x} e^{i(kx-\omega t)}. \tag{3.13}$$

In this equation, the second exponential, $e^{i(kx-\omega t)}$, is identical to the exponential expression in Eq. (3.12) and describes the harmonic behavior. The first exponential, $e^{-\alpha x}$, describes the amplitude decay due to attenuation. If one considers two stress amplitudes, $S_1 = \sigma_0 e^{-\alpha x_1}$ and $S_2 = \sigma_0 e^{-\alpha x_2}$, dividing S_2 by S_1 yields the equation

$$\frac{S_2}{S_1} = e^{\alpha(x_1 - x_2)} \tag{3.14}$$

or solving for α:

$$\alpha = \frac{1}{\Delta x} \ln\left(\frac{S_2}{S_1}\right) \quad \text{Np/unit length} \tag{3.15}$$

where $\Delta x = x_1 - x_2$. Intrinsic attenuation, as described in the above equations, is caused by both the properties of the bulk material in which the wave propagates and the properties of any inhomogeneities in the material that cause scattering of the signal. Extrinsic attenuation is due to the method of measurement. These causes of attenuation will be described in the following sections.

3.2.1 Material absorption

Dissipation of acoustic energy due to absorption in the bulk media is due to three basic types of losses: viscous losses, heat conduction losses, and losses associated with molecular exchanges [23]. In a viscoelastic media, material absorption is dominated by viscous losses—which can be thought of as frictional losses—and heat conduction losses—which result from heat transfer along temperature gradients. While an elastic material stores energy without dissipation during deformation, viscoelastic materials have

combined properties of both an elastic solid and a dissipative viscous liquid meaning there is dissipation through absorption in the conversion of energy. For these materials, stress and strain are no longer single-valued functions of one another for a complete cycle of oscillatory stress—stress is a function of both strain and the time derivative of strain. The non-linear stress-strain behavior causes a hysteresis effect between the stress and the strain. Temperature gradients can occur between regions of compression and rarefaction, and the heat transfer between regions of high and low temperatures leads to irreversible energy loss or attenuation through the production of entropy. Attenuation due to material absorption is considered to be linearly proportional to the frequency.

3.2.2 Scattering

Scattering, the second cause of intrinsic attenuation, arises in heterogeneous materials at interfaces with different acoustic properties. Grain boundaries, crystal defects, precipitates, and multiple phase inclusions can all give rise to scattering interfaces. In general, any inhomogeneity in the material has the potential to cause wave scattering, however, the ratio of the scatterer size to the wavelength determines the significance of its effect on total attenuation.

If only a single scatterer exists in the bulk material, there is only a single interaction to cause scattering, and the effect is known. For low scattering densities, interactions between scatterers are negligible, and it can be assumed that the loss caused by a single scatterer is unaffected by additional scatterers. In this case, each scatterer is treated

independently, and the total scattering attenuation is a summation of the effects of each scatterer. As the density of scatterers increases, the probability of each scattering event occurring independently of another decreases, and the interactions between scatterers cannot be ignored.

Three domains have been defined to approximate the scattering effect as a function of frequency or wavelength [24]. As mentioned previously, the significance of the effect is determined by the ratio of the scatterer radius, a, to the wavelength, λ.

Rayleigh Domain: $\alpha_s(a, \mathrm{f}) \sim f^4 \cdot a^3$ for $\frac{2\pi a}{\lambda} \ll 1$

Stochastic Domain: $\alpha_s(a, \mathrm{f}) \sim f^2 \cdot a^3$ for $\frac{2\pi a}{\lambda} \approx 1$

Geometric Domain: $\alpha_s(a, \mathrm{f}) \sim a^{-1}$ for $\frac{2\pi a}{\lambda} \gg 1$

In other words, when the radius of the scatterer is much smaller than the wavelength, the frequency dominates the attenuation more so than the scattering radius. For scattering radii on the same scale as the wavelength, the influence of the radius on the attenuation is greater than that of the frequency. Finally, if the radius of the scatterer is much larger than the wavelength, the attenuation is only a function of the scattering radius.

3.2.3 Diffraction effects

Geometric spreading, or beamspreading, is the most significant cause of extrinsic attenuation to be considered for this research. For an ideal half-space with an infinite wave source, the wave propagates through the half-space as a plane wave, i.e. no beamspreading occurs. However, as soon as a finite source is introduced, as is the case

for a pressure wave field emitted from any real transducer, the wave will begin to diverge from plane wave behavior. In other words when the wavelength is no longer negligible with respect to the source size, the beam broadens and the received signal amplitude decreases with propagation distance [25]. The radiation pattern is a function of the ratio of the wavelength, λ, to the transducer diameter, d, and the diffraction effects are therefore a function of the ratio of the wavelength to the transducer diameter and the propagation distance. Figure 3.2 shows a polar representation of the radiation patterns for three different d/λ ratios. It should be observed that increasing the d/λ ratio decreases

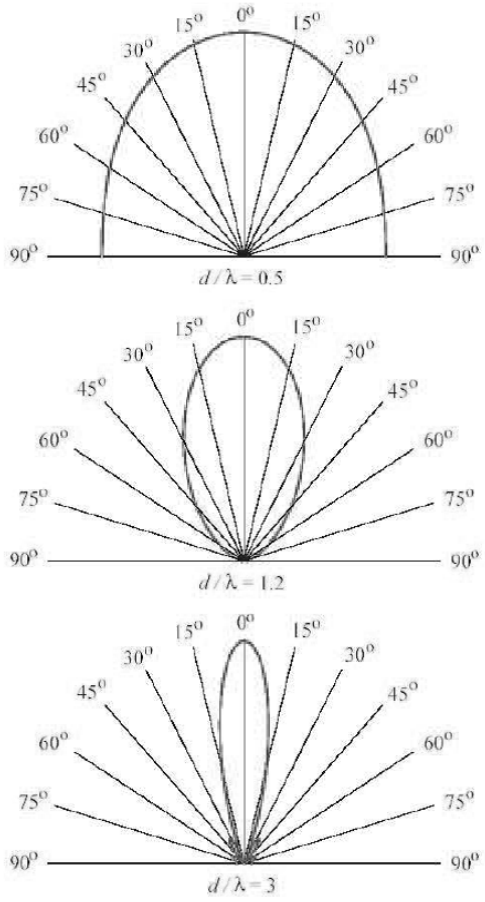

Figure 3.2: Radiation patterns of pressure waves for varying d/λ ratios [4]

the divergence of the beam—or as the wavelength becomes negligible compared to the transducer diameter, so too do the diffraction effects become negligible.

If left unaccounted for, the diffraction effect can cause considerable errors in attenuation measurements. The diffraction correction for a plane circular piston source of radius, *a*, according to Rogers and Van Buren, can be defined as the integral of the piston field area over the surface of the receiver a distance, *x*, from the transducer [26]. Both Rogers and Van Buren [26] and Lévêque, Rosenkrantz, and Laux [25] were able to derive an analytical expression for this aforementioned diffraction correction coefficient

$$D(s) = 1 - e^{-i(2\pi/s)}\left[J_0\left(\frac{2\pi}{s}\right) + iJ_1\left(\frac{2\pi}{s}\right)\right] \tag{3.16}$$

where *s* is the normalized propagation distance given by

$$s = \frac{\lambda x}{a^2} \tag{3.17}$$

and J_0 and J_1 are Bessel functions of the zeroth and first order, respectively. Using Eq. (3.16), the attenuation can now be written as

$$\alpha = \frac{1}{\Delta x}\left[\ln\left(\frac{|S_2|}{|S_1|}\right) - \ln\left(\frac{D(x_2)}{D(x_1)}\right)\right] \tag{3.18}$$

3.2.4 Attenuation in cement paste

In cement paste, intrinsic attenuation is caused by both absorption in the bulk paste and scattering due to air voids. The total intrinsic attenuation is found to be the addition of these two effects. Based on the independent scattering model described in [4], the total attenuation, α, in a cement paste specimen is described as follows:

$$\alpha = (1 - \phi)\alpha_a + \frac{1}{2} n_s \gamma^{sca} \tag{3.19}$$

where ϕ is the volume fraction of scatterers (entrained and entrapped air voids), $\alpha_a$is the attenuation inherent to the cement paste matrix, n_s is the number of scatterers, and γ^{sca} is the scattering cross section of a single scatterer. As mentioned above, the independent scattering model does not consider interactions between scatterers, which can cause it to under predict the total attenuation. However for the following results, the total air content is below 10%, and the effects of scatterer interactions are minimal.

The volume fraction of total air, ϕ, can further be related to the radius of the scatterer and the number of scatterers based on the following equation from [4]:

$$\phi = \frac{4}{3} \pi a^3 n_s \tag{3.20}$$

where a is the radius of the scatterer. Because the absorption of the bulk matrix, α_a, and the scattering cross section, γ^{sca}, are considered constant and are fairly easily obtained, together Eq. (3.19) and (3.20) provide a useful relationship between the air void size and volume content and the ultrasonic attenuation. Figure 3.3 shows a plot of the theoretical attenuation versus frequency for increasing scatterer volume fractions for a constant scattering radius as determined by Punurai using the independent scattering model [4].

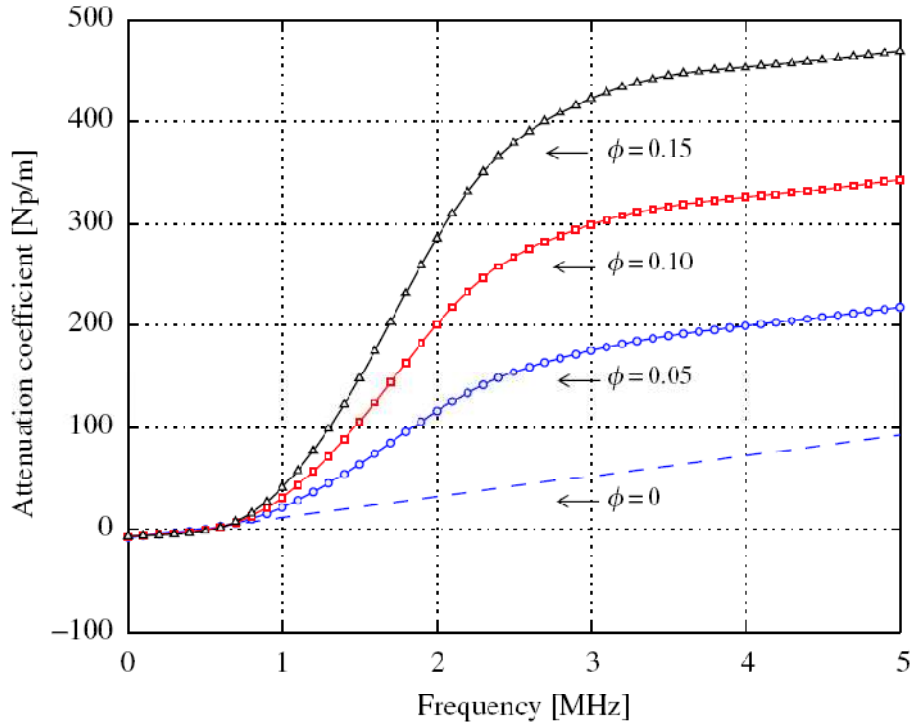

Figure 3.3: Theoretical attenuation for varying air volume fractions, a = 0.3 mm [4]

3.3 Biot's theory

Wave propagation through an elastic media has been described above including a model to account for finite, discontinuous inclusions or scatterers. However upon considering a fluid-saturated porous media, the behavior of and interaction between each of the two coexisting phases—the porous media and the pore solution—must be studied. Biot's theory for fluid-saturated porous media [27-30] can be used to describe and model acoustic wave propagation through this media.

Because there now exists two phase under consideration, let $\boldsymbol{u}$ be the mean macroscopic displacement of the material and $\boldsymbol{U}$ the mean displacement of the fluid. From this, it is natural to introduce a macroscopic stress tensor, $\boldsymbol{\sigma}$, and a mean pressure in the fluid, p. If a unit element or cube of the macroscopic material is defined, it should be noted that the average macroscopic displacement, $\boldsymbol{u}$, represents the mean displacement of this reference element as a whole, not just of the porous matrix. The liquid phase under consideration is assumed to be continuous, or in other words, the pores are assumed to be channels through which fluid flow may occur. This flow, $\dot{\boldsymbol{w}}$, can be defined as

$$\dot{w}_i = K_{ij} X_j \tag{3.21}$$

where the tensor, $\boldsymbol{K}$, can be identified with the hydraulic permeability and $\boldsymbol{X}$ represents the force on the fluid and is related to the pressure gradient. For the given system, previous work [29] has found the equations of motion to be

$$\sigma_{ij,j} = \rho \ddot{u}_i + \rho_{uw} \ddot{w}_i \tag{3.22}$$

$$-p_{,i} = \rho_{uw} \ddot{u}_i + \rho_w \ddot{w}_i + \frac{1}{K} \dot{w}_i \tag{3.23}$$

where ρ is the macroscopic density and ρ_w and ρ_{uw} are density coefficients that represent the mass coupling between fluid and solid, or the dynamic coefficients as described by Biot [27, 28]. Here the equations have been formulated for the isotropic case which allow for the definition of the scalar, K. For this provision, $\boldsymbol{K}^{-1}$ is proportional to unity, $\boldsymbol{K}^{-1} = K\mathbf{1}$.

A significant discovery by Biot in his work on fluid-saturated porous media was the existence of three waves in a porous media, two dilatational or pressure (P-) waves and

one rotational or shear wave [27, 28]. In order to determine the velocities of each of these waves, one must consider pressure waves and shear waves that satisfy

$$\begin{pmatrix} \boldsymbol{u} \\ \boldsymbol{U} \end{pmatrix} = \begin{pmatrix} \boldsymbol{grad}\ \phi_1 \\ \boldsymbol{grad}\ \phi_2 \end{pmatrix} = \boldsymbol{curl}\ \boldsymbol{\Phi} \tag{3.24}$$

and

$$\begin{pmatrix} \boldsymbol{u} \\ \boldsymbol{U} \end{pmatrix} = \begin{pmatrix} \boldsymbol{curl}\ \boldsymbol{\Psi_1} \\ \boldsymbol{curl}\ \boldsymbol{\Psi_2} \end{pmatrix} = \boldsymbol{curl}\ \boldsymbol{\Psi} \tag{3.25}$$

respectively. For the dilatational case, it is found that

$$\boldsymbol{R}\nabla^2\boldsymbol{\Phi} - \boldsymbol{M}\ddot{\boldsymbol{\Phi}} = 0 \tag{3.26}$$

where $\boldsymbol{R}$ and $\boldsymbol{M}$ are the rigidity and mass matrices respectively. There are two real positive roots or eigenvalues that satisfy Eq. (3.26), and these correspond to $V_{P_1}^2$ and $V_{P_2}^2$. The wave corresponding to the velocity V_{P_1} is considered to be a true wave, and describes the in-phase movement of the overall element and the fluid. The wave corresponding to $V_{P_2}$is called the slow wave drawing from the fact that V_{P_2} is significantly lower thanV_{P_1}. The slow wave is produced by out of phase motion between the overall element and the fluid and is said to be highly dispersive and attenuated. For the shear case, it is found that

$$\nabla^2\boldsymbol{\Psi}_1 - \frac{1}{V_s^2}\boldsymbol{\Psi}_1 = 0$$

$$\boldsymbol{\Psi}_2 = -\left(\frac{\rho_{12}}{\rho_{22}}\right)\boldsymbol{\Psi}_1 \tag{3.27}$$

where ρ_{12} and ρ_{22} are entries in the mass matrix, $\boldsymbol{M}$, and V_s^2 is the corresponding velocity of the rotational or shear wave. The motion of the fluid associated with this shear wave is in phase with the movement of the overall element.

CHAPTER 4

EXPERIMENTAL PROCEDURE

In the application of ultrasonic methods for the characterization of fresh cement paste, one of the most limiting problems faced by previous researchers [11, 31] was the need of a containment vessel due to the specimen's lack of rigid form. This research arrived at a completely new approach that takes advantage of the amorphous, fluid nature of plastic cement paste. This section will describe the immersion technique developed as well as the overall experimental setup.

4.1 Ultrasonic experimental setup

The experimental setup used in conducting the ultrasonic measurements is shown in Figure 4.1. Below, the ultrasonic equipment and exact experimental procedure are described in detail.

4.1.1 Ultrasound equipment

Pulser: A Panametrics NDT 5058PR pulse generator is used as the signal source. The pulser is connected to both the oscilloscope and the piezoelectric transducer, sending the trigger signal to the oscilloscope and the electrical impulse to the transducer. The use of an impulse signal excites a wide range of frequencies and

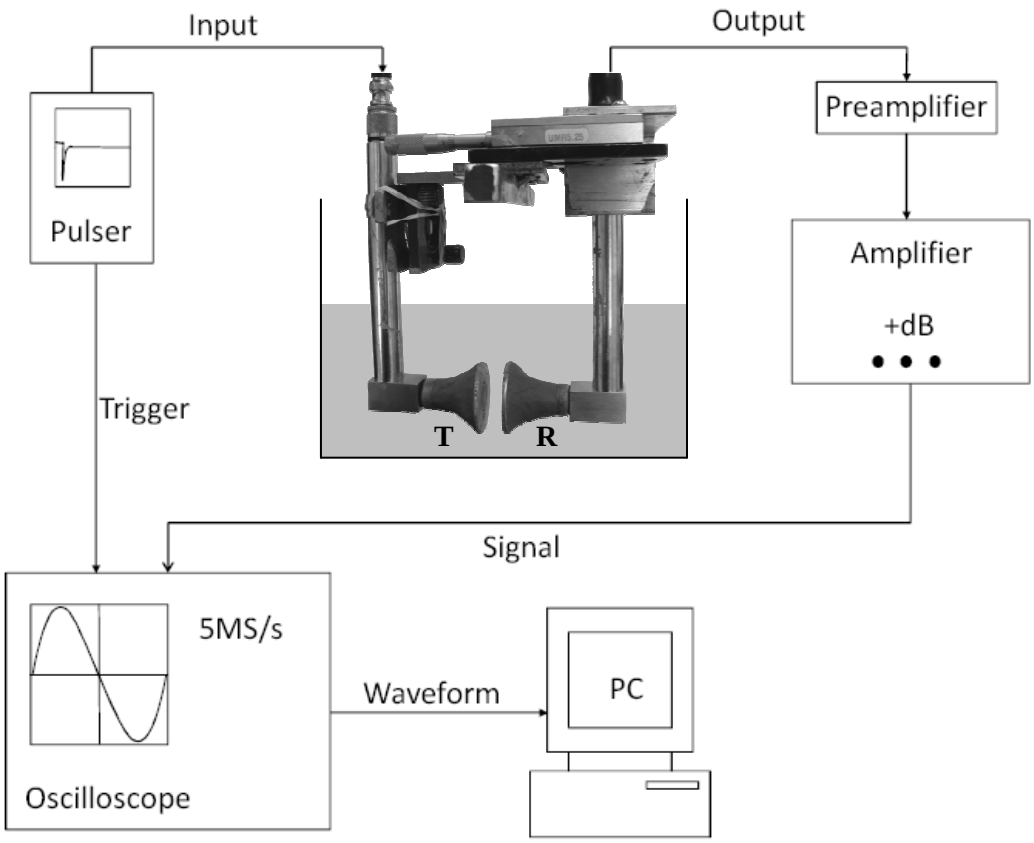

Figure 4.1: Schematic of ultrasonic experimental setup

allows for broadband performance of the transducers. An electrical impulse of 400 V is used in order to input sufficient energy to detect an output signal with an acceptable signal-to-noise ratio. Any higher input energy could potentially be harmful to the ultrasonic equipment. The pulser repetition rate for the signal was chosen to be 2 kHz, which is the highest available with this pulser. This minimizes the time required for averaging and recording a given signal.

Piezoelectric transducers: A pair of Panametrics V303 broadband immersion transducers with center frequency and radius of 1 MHz and 1.27 mm respectively are used for the experimental setup. Later it will be seen that in the early stages of hydration, the fresh cement paste acts as a filter for frequencies above 200 kHz. However the transducer frequency was chosen based on the approximate size of the scatterers to be detected. The impulse is sent from the pulser to the transmitting transducer where the piezoelectric element converts the electrical signal to mechanical energy or in this case to a longitudinal stress wave. The receiving transducer detects the longitudinal wave after the wave travels through the fresh cement paste.

Pre-amplifier and amplifier: Both a pre-amplifier and an amplifier are used to increase the signal-to-noise ratio. The signal is first processed by a Digital Wave PA2040G/A preamplifier that allows for discrete amplification by -20 dB, 0 dB, +20 dB, or +40 dB. It is then processed by a Digital Wave FTM4000 amplifier/receiver which can provide an additional +42 dB of amplification through a +21 dB switch and another +21 dB in +3 db increments. In the earlier stages of hydration and at further separation distances, the signal can be especially difficult to detect and monitor. The use of both the preamplier and amplifier/receiver allows for precise control of the recorded signal amplitude and signal-to-noise ratio. Waveforms are adjusted during signal processing to correct for different levels of amplification. However, amplification levels are held constant between two measurements to be compared for phase velocity and attenuation calculations.

Oscilloscope: Finally, the signal travels from the amplifier/receiver to the Tektronix TDS5034 oscilloscope where is can be displayed and recorded. The sampling frequency (resolution), sample length, and signal averaging are user specified through the oscilloscope. The oscilloscope also allows for monitoring of the signal in the time domain before the waveform is recorded and saved. Increasing the voltage scale of the displayed waveform provides for secondary adjustment to the signal-to-noise ratio and overall waveform resolution.

4.1.2 Immersion apparatus

In order to collect and record ultrasonic waves in fresh cement paste, a thru-transmission technique is used. For solid specimens such as hardened cement paste or steel, transducers can be mounted directly to the sides of the material to generate and detect the waveforms as shown in Figure 4.2 [6]. However because fresh cement paste lacks the

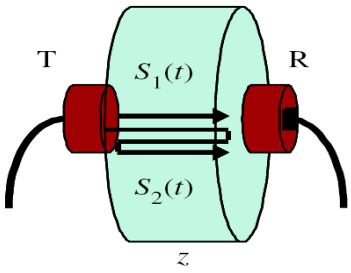

Figure 4.2: Common thru-transmission setup for solid specimens [6]

rigidity to form a solid, cohesive shape, this approach must be adjusted, and a containment vessel is clearly needed to restrain the material. Previous researchers [7-10, 11, 31] fixed the transducers to the outside of Plexiglas containment vessels in order to

overcome the issues brought on by the amorphous nature of the paste. Figure 4.3 shows the experimental setup used by Aggelis and Philippidis [31] to measure wave propagation through fresh cement paste. The setup used by Kmack [11] is nearly identical.

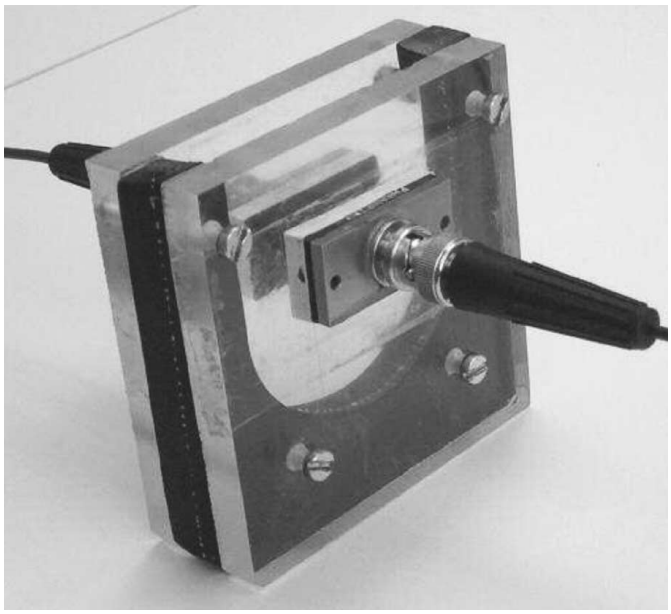

Figure 4.3: Plexiglas containment vessel with transducer fixed outside the plates [31]

A few serious concerns arise with the aforementioned experimental setup. Because the waves are traveling through a Plexiglas plate before and after propagating through the cement paste, additional interfaces are introduced upon which some reflection inevitably occurs. In order to compare two signals traveling through distinct propagation distances, the thru-transmission signal is compared to the twice-reflected signal whose propagation distance is three times the plate separation. In this setup, the number of encounters with the Plexiglas interfaces for the twice-reflected wave is greater than that for the thru-transmission signal. Due to this, the measured attenuation will be higher than the true attenuation on account of losses at the additional Plexiglas interfaces. Additionally due

to the reliance on the reflected waveform, the propagation distance of the second signal must be three times that of the first thru-transmission signal. Because the fresh cement paste is so highly attenuative, especially at early ages, the propagation distance is very limited; at longer propagation distances, the signal is completely attenuated out. In order to detect a clear reflected signal with a sufficient signal-to-noise ratio, the transducers must be moved very close together. However as separation distance between the Plexiglas plates decreases, the reflected signal is no longer separable from the thru-transmission signal because the arrival times of the two wave paths both approach zero. Furthermore, diffraction corrections become more critical as the transducers are moved even closer in the near field.

These issues associated with the previous methods for measuring ultrasonic attenuation in fresh cement paste provided the motivation to develop a new immersion setup. With the immersion apparatus, the transducers are immersed directly in the fresh cement paste; the paste surrounds the apparatus and is in direct contact with the transducer faces. Therefore, the paste can be confined by any containment vessel so long as it's sufficiently large enough to fit the apparatus and provide adequate spacing between the transducers and the vessel walls so that reflections off the walls do not interfere with the thru signal. Instead of relying on a reflected signal to record two waveforms with distinct propagation paths, the immersion apparatus takes advantage of the plastic state of the cement paste. The transducers are moved between measurements to record two thru-transmission signals having different propagation distances. This also eliminates the need for reflection coefficient adjustments.

Figure 4.4 shows the immersion apparatus conceived, designed, and built exclusively for this research. The metal washers and green clay denoted by box A serve two purposes for the device. As the hydration of the cement paste proceeds, it is common for water to separate from the mix and rise to the surface of the cement paste. There was concern that this bleed water was collecting on the bottom face of the transducer and, with time, rising and forming a water film upon the transducer face. The washers and clay provide a more

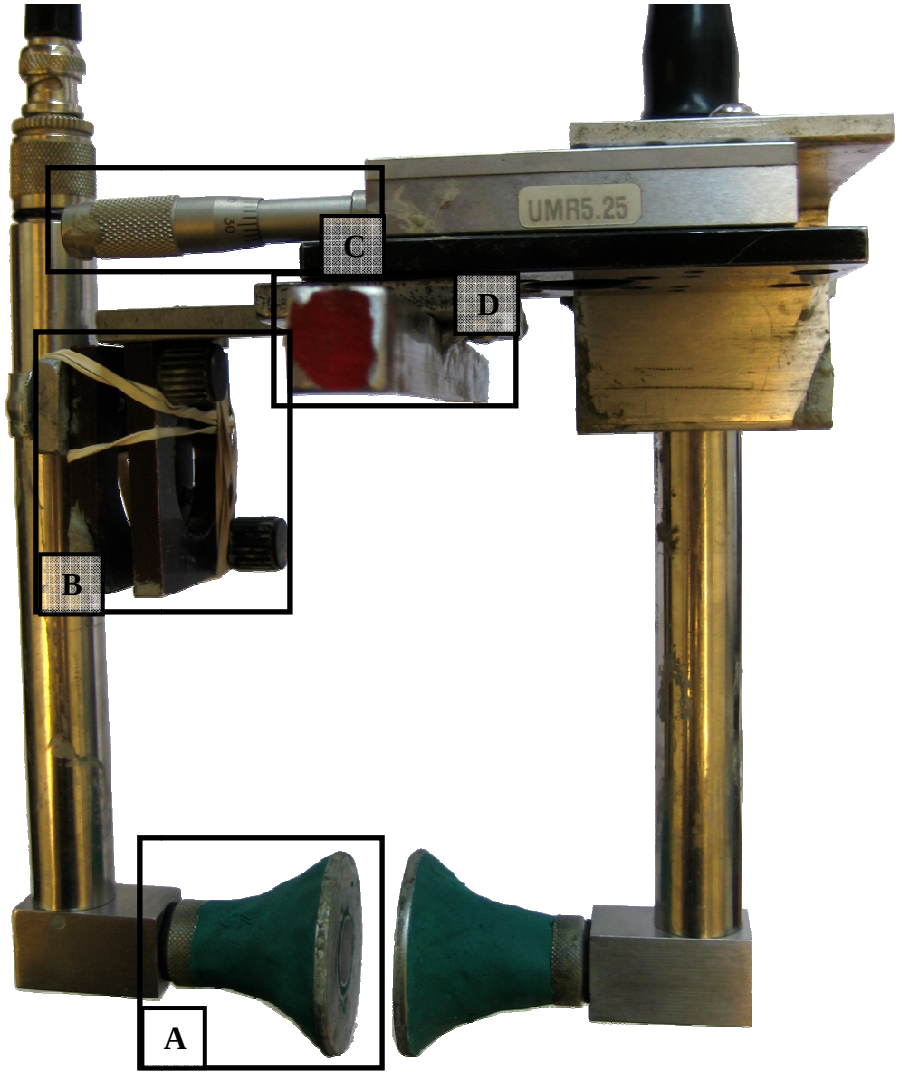

Figure 4.4: Ultrasonic immersion apparatus

favorable path for the bleed water that prevents it from possibly collecting along the transducer face as shown in Figure 4.5. The second benefit is associated with the diffraction correction and beam spreading consideration. The diffraction correction discussed previously for use in the attenuation calculation assumes that the propagating

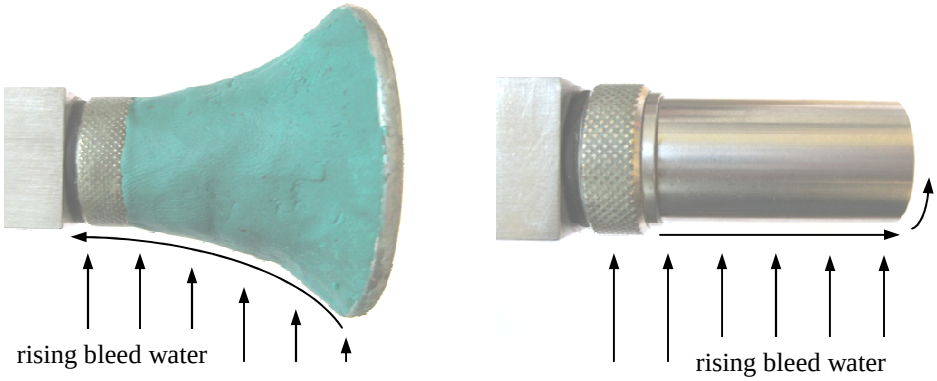

Figure 4.5 Path of rising bleed water with and without washer

waveform is a plane wave. When a transducer is mounted on a plane surface, this assumption is fairly accurate. However in the absence of the washers, the bulk material through which the wave propagates surrounds all surfaces of the transducer, which brings into question the plane wave assumption. The washers help simulate a plane of incidence, or in other words, the bulk cement paste better approximates a half-space. The angle adjustor, denoted by box B, ensures that the two transducer faces are parallel to each other. Box C indicates the micrometer which is used to accurately measure the separation distance between transducers. Finally, box D outlines the long rectangular rod by which the entire immersion apparatus is suspended from the containment vessel.

4.1.3 Measurement procedure

Prior to mixing, the immersion apparatus is suspended from the containment vessel by the rectangular rod and secured with clamps. For the current setup, a plastic containment vessel measuring about 102 mm by 254 mm is used. Once the paste specimen is mixed, it is placed in the containment vessel. The paste is consolidated through the use of a vibration table, and after which, it surrounds the transducers. This process is completed systematically so that the ultrasonic signals through the paste can be monitored as early as 20 minutes after mixing.

The sequence used to collect the data for calculating phase velocity and attenuation is portrayed in Figure 4.6. In order to find phase velocity and attenuation, as given by Eq. (3.18), an ultrasonic signal, S_1, is recorded for a separation distance, x_1. Subsequently,

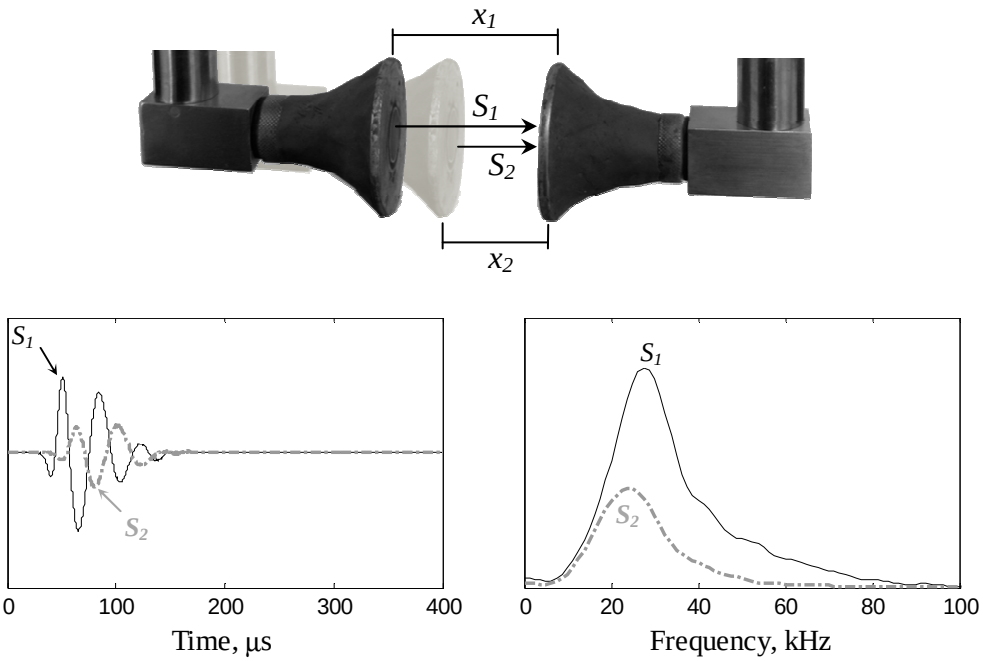

Figure 4.6: Portrayal of phase velocity and attenuation measurement procedure

the transducers are moved closer together through adjustment of the micrometer, and a second ultrasonic signal, S_2, is recorded for a shorter separation or propagation distance, x_2. The acquisition of S_2 is begun 20 seconds after the acquisition of S_1 was initiated. By comparison of the frequency domain of each of the two signals, S_1 and S_2, the ultrasonic phase velocity and attenuation can be found. The following equation is used to calculate phase velocity:

$$c = \frac{2\pi f * (x_1 - x_2)}{\left| arg\left(\frac{S_2}{S_1}\right)\right|} \tag{4.1}$$

where $\left| arg\left(\frac{S_2}{S_1}\right)\right|$ indicates the magnitude of the unwrapped phase of the complex number. Computationally, this term, $\left| arg\left(\frac{S_2}{S_1}\right)\right|$, is found by taking the absolute difference in phase angles of the two signals. Again, the attenuation coefficient is calculated using the below equation from Chapter 3

$$\alpha(f) = \frac{1}{x_1 - x_2}\left[\ln\left(\frac{|S_2|}{|S_1|}\right) - \ln\left(\frac{D(x_2)}{D(x_1)}\right)\right] \tag{4.2}$$

where D(x) is the diffraction correction given by Eq. (3.16).

Phase velocity and attenuation were initially calculated at 40, 45, and 50 minutes after mixing for a single sample. However, in later tests designed to compare attenuation for pastes with varying levels of air entraining admixture (AEA), the phase velocity and attenuation were only calculated at 40 minutes after mixing. While the signal strength and signal-to-noise ratio improve with time, the viscosity of the paste also increases with time. Moving the transducer at later ages increases the risk of permanently disturbing the bulk cement paste because the paste loses its ability flow back to the undisturbed state.

4.1.4 Coupling issues

In order to accurately measure phase velocity and attenuation, the coupling conditions and the state of the bulk media for the first and second recorded waveforms should ideally be identical. However upon studying the initial waveforms before and after the transducers were moved, the apparent arrival velocity appears to drop after the separation distance was changed. This will be discussed further in the results chapter that follows. Moving the transducers potentially changes the coupling at the transducer-cement paste interface. Therefore in order to more closely approximate identical coupling between the first and second waveforms, the transducers are moved 20 seconds before the first waveform acquisition is to begin. In other words to record the data for the attenuation calculation at 40 minutes, the transducers are first moved closer, to the separation distance x_1, at 39 minutes and 40 seconds. At 40 minutes, the signal S_1 is recorded, and the transducers are moved to the separation distance x_2. Finally at 40 minutes and 20 seconds, the acquisition of S_2 begins.

4.2 Cement paste specimens

All specimens were prepared using an ASTM Type I Portland cement [32], produced by Lafarge. The chemical composition of this cement based on x-ray florescence according to ASTM C114 [33], including potential compositions based on a Bogue oxide analysis, is provided in Table 4.1. The w/c for each mix design remained constant at 0.35. This

Table 4.1: Cement composition

Compound	Amount (%)
C_3S*	54.74
C_2S*	17.40
C_3A*	7.25
C_4AF*	9.74
CaO	62.71
SiO_2	20.41
Al_2O_3	4.78
Fe_2O_3	3.20
MgO	3.17
SO_3	3.07
K_2O	0.56
TiO_2	0.25
Mn_2O_3	0.14
Na_2O	0.06
P_2O_5	0.06
SrO	0.03
Cr_2O_3	0.02
ZnO	0.01

* Composition based on Bogue oxide approximation

w/c is relatively low, but was chosen to reduce bleeding effects while still remaining representative of modern concrete mixtures. The changing variable across the five different mixes is the level of chemical air entrainer. The air entrainer used for this research is BASF MB-AE 90, which is an anionic surfactant derived from rosin. The level of air entrainer varies from 0% up to 0.8% AEA by mass of cement, and two replicate specimens are tested for each level of AEA. BASF recommends anywhere between 0.02-0.25% AEA by mass of cement to entrain 2-4% air in a given concrete mix. Considering that air void systems are more stable in concrete than cement paste, the increased dosages of air entrainer were chosen to compensate for the additional

instabilities present in the cement paste void system. While the two samples for each level of AEA were identical in mix design, they were mixed and tested on separate occasions. However, the temperature remained fairly constant at 25.0ºC±0.5ºC during mixing, and many precautions were taken to ensure an identical mixing procedure. Therefore, the replicate mixes should be nearly identical. The initial separation distance varied from 14-15 mm and the second transducer separation distance varied from 10-13 mm.

Table 4.2 summarizes the details for each specimen. The air volume fractions were determined according to ASTM C 457 Procedure B—Modified Point-Count Method. For this test method, the sample is examined under a microscope, and the phase (void, paste, aggregate) observed at each point along a line of the sample is recorded. The air content is determined by dividing the number of points that coincided with an air void by the total

Table 4.2: Specimen specifications

Name	w/c	% AEA	Air fraction (% by volume)
CP01	0.35	0.0	-
CP02	0.35	0.0	0.6% *
CP03	0.35	0.1	-
CP04	0.35	0.1	2.0% *
CP05	0.35	0.2	-
CP06	0.35	0.2	2.3% *
CP07	0.35	0.4	-
CP08	0.35	0.4	4.2% *
CP09	0.35	0.8	-
CP10	0.35	0.8	2.1%, 6.2% *, [a]

*As examined by a trained petrographer according to ASTM C 457 B [19]
[a] Poor distribution of the voids resulted in half of the sample having a smaller volume fraction

number of points along the line. According to the petrographic analysis, the air content generally follows the expected trend of increasing air with increasing AEA. However between CP04 and CP06, the observed increase in air volume was not substantial considering the dosage of AEA doubled. Additionally for CP10, the void distribution of the sample was not uniform, as about half of the examined surface had an air fraction around 2%, while it was over 6% for the other half. It is possible that these inconsistencies in air content could have affected the ultrasonic results, especially if the paste between the transducers experienced local air void distributions differing from that of the overall sample.

4.2.1 Mixing procedure for ultrasonic testing

While wave propagation through fresh cement paste changes with level of hydration, the time after mixing is used as the parameter to approximate hydration levels. Therefore, in order to best simulate equivalent hydration levels at a given point in time, the mixing procedure is performed with a very precise schedule for the occurrence of each event. In preparation for ultrasonic testing, mix ingredients are measured to an accuracy of 0.01 g. The cement is then added to the water (and air entrainer) which requires about a minute due to the considerable batching size. From 1:15-2:30, the mixture is hand blended to wet the cement. A planetary mixer is used to provide further blending according to the following steps: 2:45-3:15 (30 seconds) mixing on the low speed, 3:15-4:00 scraping of the side and bottom of the mix bowl, 4:00-5:00 (60 seconds) mixing on medium speed. The paste is then poured into the plastic containment vessel to surround the immersion

transducers, already suspended from the top of the container. In order to minimize vibration while still ensuring the paste completely surrounds the transducers, the paste is added to the container to a level which partially covers the transducers before the paste is vibrated using a vibration table for 10 seconds. Then, the second portion of paste is added to the container, and the paste is vibrated for an additional 10 seconds. The minimization of total vibration to only 20 seconds was chosen to prevent the removal of entrained air.

4.3 Waveform acquisition and signal processing

4.3.1 Signal digitization

In order to record and save real waveforms, the information must be compressed by means of digitization of the analog signal. To accurately preserve the properties of the waveform, appropriate sampling parameters must be chosen. Aliasing is one potential effect that can distort the digitized waveform. If the sampling interval, Δt, is too large compared to the signal period, T, then the periodicity of the digitized signal appears to be larger than that of the true waveform. Therefore, the sampling rate or frequency, $f_s = \frac{1}{\Delta t}$, should be greater than or equal to the Nyquist frequency, $f_{ny} = \frac{2}{\mathrm{T}}$. A second sampling parameter to be considered is the number of waveforms over which the signal is averaged. Signal averaging can reduce the interference caused by unpredictable noise and variance inherent to electronic signals, thereby improving the signal-to-noise ratio.

However due to the time dependent nature of the fresh cement paste, signal averaging must be completed in a sufficiently short period of time.

In the ultrasonic tests conducted for this research, a sampling frequency of 5 MHz was chosen to sample 2000 points, providing for a total window length of 400 µs. The number of waveforms averaged varied from 1,000 up to 10,000 signals, however, the higher number of averages was only used for signal acquisition at early times. The averaging of 10,000 waveforms lasts close to 40 seconds, which is not insignificant when measuring two signals to compare for the purpose of calculating ultrasonic attenuation. Therefore when taking the two measurements 20 seconds apart in order to calculate phase velocity and attenuation, only 1,000-2,000 waveforms are averaged. This averaging requires less than 10 seconds, which allows for signal averaging, data saving, and moving of the transducers in time to begin the second acquisition 20 seconds after the first.

4.3.2 Windowing

A rectangular window is used to isolate the true waveform from the overall recorded signal. The rectangular window was chosen over a different windowing function such as a Hanning or Hamming window to decrease any potential distortion or concentration of the signal energy. As seen from Figure 4.7, the windowing for air entrained signals is relatively straight forward due to the existence of only a single wave. However for the non-air entrained signals, windowing proved to be much more challenging. Figure 4.8 shows a typical non-air entrained signal prior to and after windowing. As will be

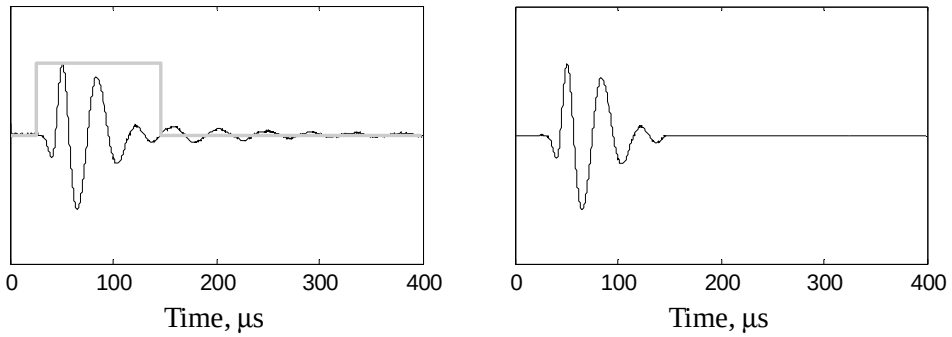

Figure 4.7: Windowing of typical air entrained specimen

discussed in Chapter 5, signals through non-air entrained specimens consist of two distinct waves. While the second wave is believed to contain the desired information, it is difficult to window out the first wave.

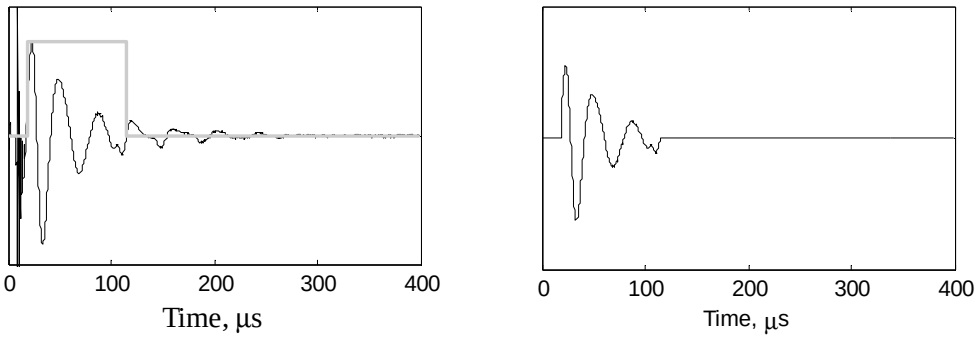

Figure 4.8: Windowing of typical non-air entrained specimen

CHAPTER 5

RESULTS AND DISCUSSION

5.1 Ultrasonic results

Ultrasonic tests were performed to observe the time and frequency domain signals and to measure ultrasonic phase velocity and attenuation as a function of different paste parameters. The results from these ultrasonic tests are summarized below.

5.1.1 Non-air entrained vs. air entrained

The first observation noted during initial testing was the existence of two different waves in the non-air entrained fresh paste, each having a very different signal strength and frequency. These two waves are easily distinguished in the 0.30 water-to-cement ratio (w/c) paste, as seen in Figure 5.1. The first, faster wave has a much higher amplitude and frequency. The second wave arrives later and is very highly attenuated when compared to the first. Similar to the 0.30 w/c samples, the non-air entrained mixes with a w/c of 0.35 also appeared to have these two types of waves. Figure 5.2 shows the first and second waves in the 0.35 w/c non-air entrained fresh cement paste. In contrast to non-air entrained specimens with a w/c of 0.30, it is clear that the arrival time of the second wave for the 0.35 w/c paste is not sufficiently different from that of the first wave, so that the two waves are not visually distinct and separated in the time domain.

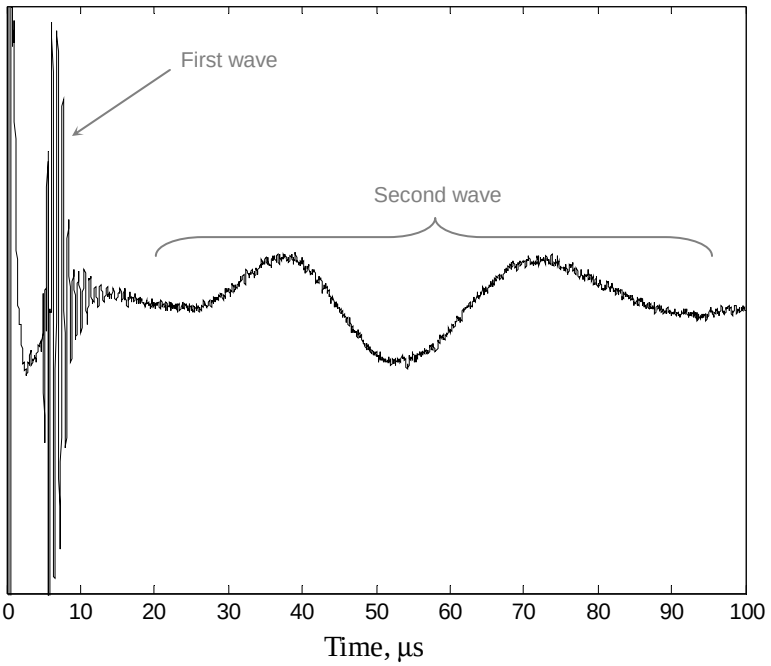

Figure 5.1: Signal through 0.30 w/c non-air entrained paste

Besides the difference in arrival time of the second wave, there is a clear difference in the ratio of signal amplitudes of the first and second waves between the two w/c's. For the first hour of hydration, the difference in signal strength between the two waves for a 0.35 w/c cement paste is so great that it proved impossible to accurately display both signals in a single time-domain measurement. Figure 5.2 (a) and (b) had to be recorded with different acquisition parameters in order to capture each of the desired features because such a high level of amplification is required to accurately display the second wave, that the first wave becomes distorted and clipped by the oscilloscope. However, this difference in signal strength between the first and second wave is not nearly as extreme for the 0.30 w/c paste. It can be seen that the ratio of amplitudes of the first wave to the second wave is greater for the 0.35 w/c paste, versus the 0.3 w/c paste.

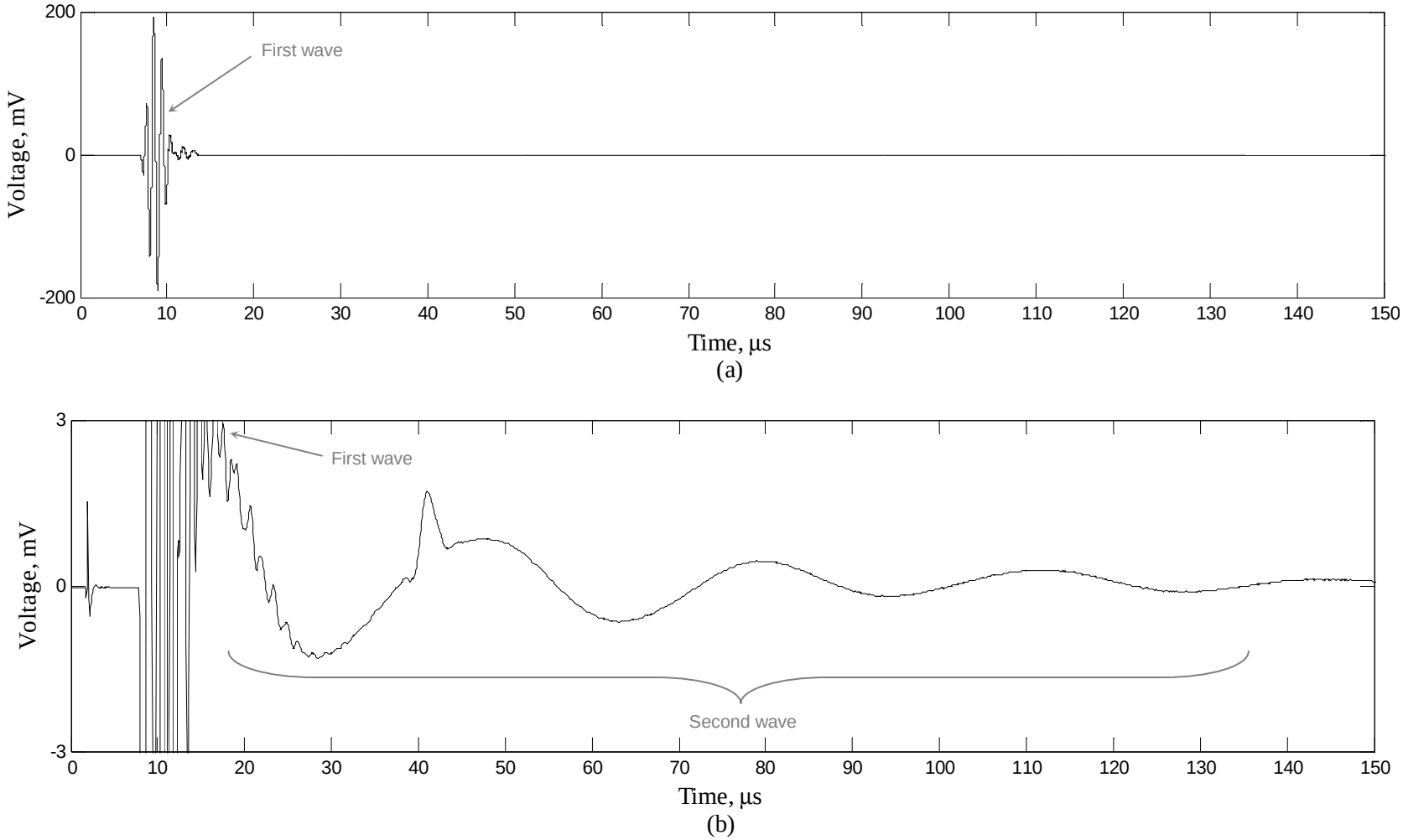

Figure 5.2: Signal through 0.35 w/c non-air entrained paste (a), and close up of second wave (b)

In other words, the amplitude of the first wave in relation to that of the second wave is larger for the mix with a larger fraction of water. This supports the hypothesis further developed below that the non-air entrained paste consists of two phases, possibly a solid porous matrix and fluid filled pores, with an aqueous or water dominant phase or pore solution.

In order to better understand the first and second waves in non-air entrained pastes, it is desirable to not only compare them in the time domain, but also in the frequency domain. While the time domain signals suggest that the two waves have considerably different frequencies, this is much clearer through a comparison of the frequency spectra. Figure 5.3 shows the frequency spectra of the first and second waves in a 0.35 w/c non-air entrained fresh cement paste. The center frequency of the first wave is close to 1 MHz, which is the resonance frequency of the transducers. In fact, the frequency response of

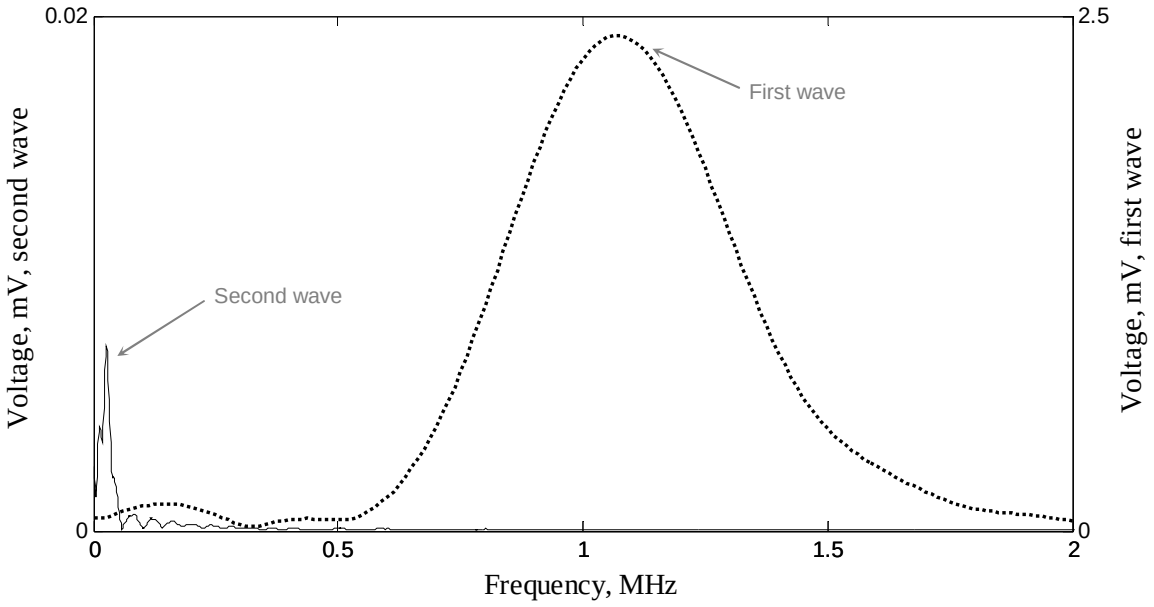

Figure 5.3: Frequency spectra for the first and second waves in non-air entrained pastes

the first wave overall is quite similar to that of the transducer. Because this first wave is not very attenuative or dispersive, it does not appear to be incredibly sensitive to the overall properties of the fresh cement paste. In contrast to the first wave, the slower second wave appears to be highly attenuative and dispersive. Its frequency spectrum is drastically shifted to the left or lower frequencies with a center frequency around 30 kHz. Its propagation path seems to effectively filter out frequencies above 200 kHz.

Figure 5.4 shows the phase velocities as calculated by Eq. (4.1) for each of the two non-air entrained waves. The first wave has a phase velocity close to that of water, which is 1600 m/s, while the phase velocity of the second wave is about an order of magnitude smaller. Note the very different frequency ranges of both signals as seen in Figure 5.3. Comparable pulse velocities were observed in the first hour of hydration by Kmack [11]. He hypothesized that the first wave travels through a liquid percolation path consisting of

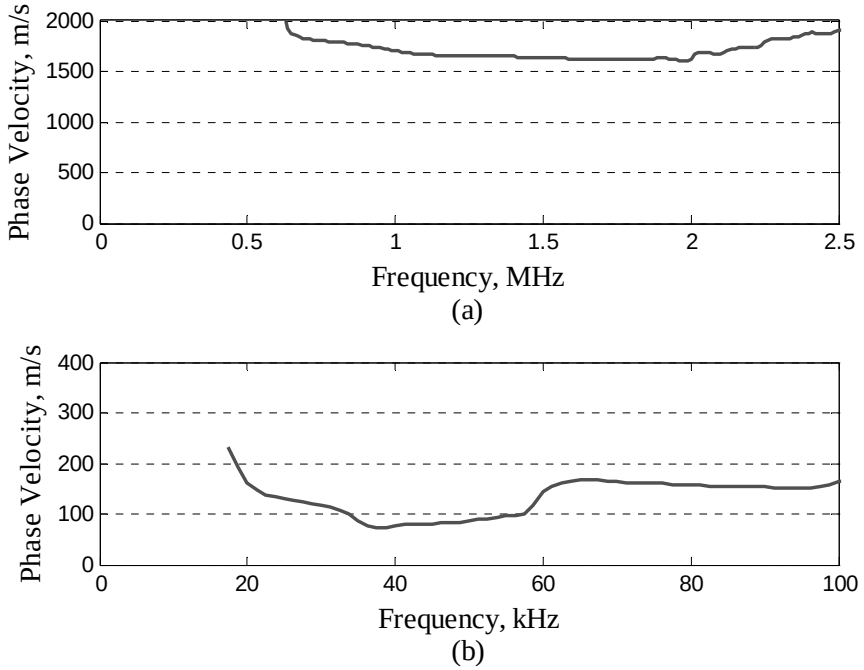

Figure 5.4: Phase velocities for first (a) and second (b) wave in non-air entrained paste

free water not adsorbed by the paste matrix. The second wave, therefore, is considered to be traveling through the bulk paste or matrix. If the plastic cement paste is considered on a larger scale, it does consist of a solid skeleton formed from hydration products and unhydrated cement grains, which is surrounded by an aqueous solution. Because of this, it is believed that these results for the non-air entrained paste may be explained by Biot's Theory for wave propagation in fluid-saturated porous media, described in Section 3.3. Note that Sayers and Dahlin also proposed the use of Biot's theory to described wave propagation in plastic cement paste [8]. The two waves observed in the above figures seem to follow Biot's prediction of a fast and slow dilatational wave. Following Biot's description, the second or slow wave observed in the non-air entrained paste is clearly dispersive and highly attenuative. Its phase velocity is also drastically lower than the first, or fast wave. This provides more evidence supporting the hypothesis briefly mentioned above that wave propagation through non-air entrained cement paste is characterized by the properties of both a bulk matrix material and water filled pores, and by the interactions between these two phases.

Unlike non-air entrained mixes, signals in air entrained fresh cement paste consist of only one wave. Figure 5.5 shows a comparison in both the time and frequency domains between the second wave in a non-air entrained paste and the air entrained wave. Here, it is clear that the two-wave phenomenon is unique to non-air entrained pastes. This is believed to be due to the chemical composition of the air entrainer which causes an increase in adsorption of the mix water and aids in the deflocculation or dispersion of cement particles. Due to these interactions in air entrained cement paste, it is possible

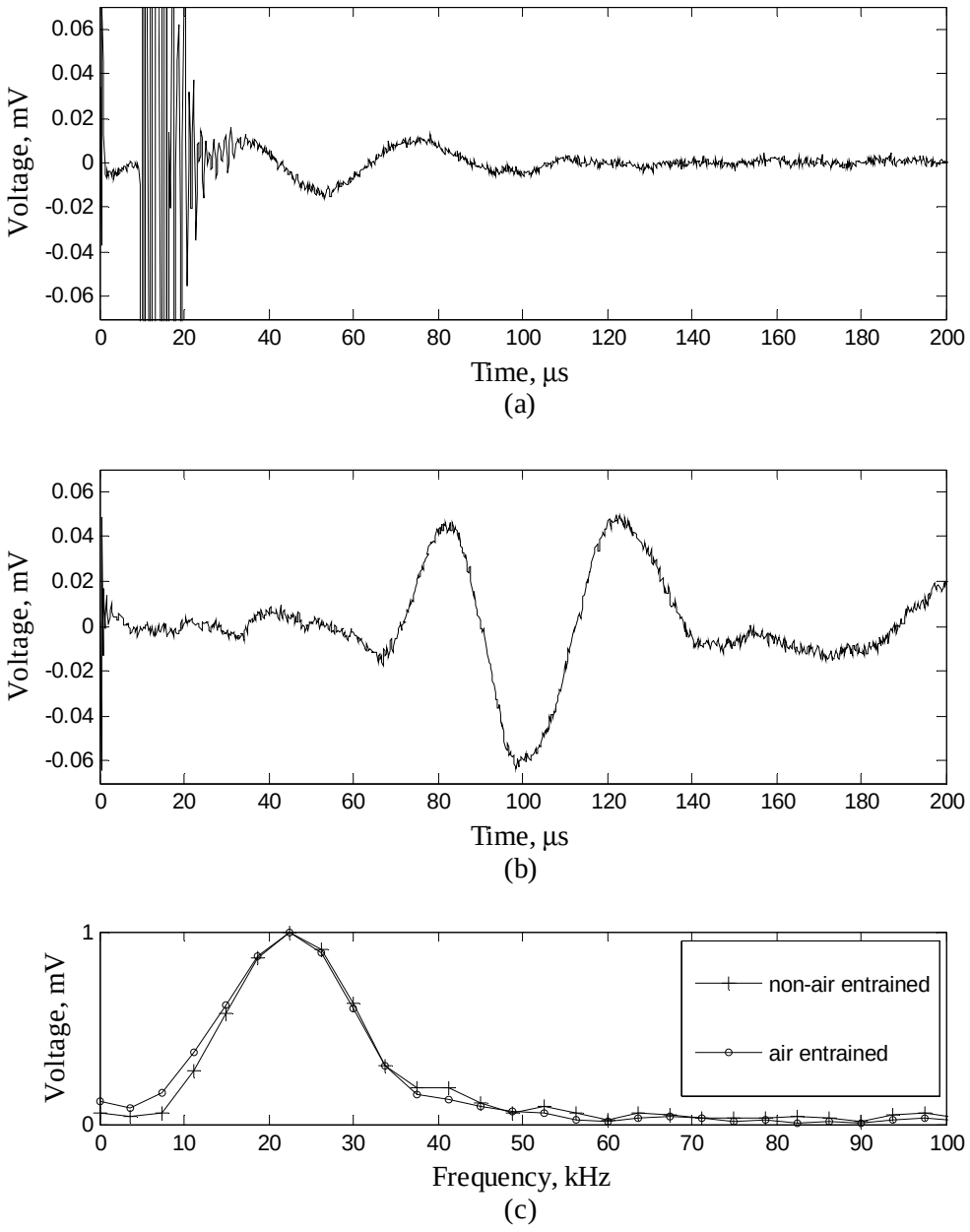

Figure 5.5: Non-air entrained (a) and air entrained (b) signals in the time, and normalized frequency spectra (c)

that the mixture as a whole behaves more like a homogeneous slurry than a suspension of solid particles in water, or a fluid-saturated porous media, which would explain the existence of only one wave. Note that in Figure 5.5 both signals were recorded at a propagation distance of 15 mm and a hydration time of 40 minutes. The single wave observed in the air entrained sample is very similar to the second, slower wave in the non-air entrained paste, but with a delayed arrival time. This behavior supports the notion that the non-air entrained slow wave and the air entrained wave represent the same propagation mode, since the normalized frequency spectra of these two waves are almost identical. The phase velocities are also similar in magnitude.

5.1.2 Variation in Ultrasonic Signals as a Function of Time

In order to better understand the behavior of the cement paste and to develop an accurate procedure for measuring and calculating phase velocity and attenuation, the waveforms were monitored during the first 50 minutes of hydration. Figure 5.6 and 5.7 show the changes in measured ultrasonic signals in both the time and frequency domains, respectively, as a function of time for CP05 at a propagation distance of 10 mm. Recall that CP05 is one of the mixes with 0.2% AEA and a w/c of 0.35. It is clear that the signal amplitude, signal frequency, and arrival time all increase with increasing hydration time or age. Note in Figure 5.7 that as the hydration time increases, the energy in the higher frequencies also increases. Therefore at later hydration times, the frequency range for which phase velocity and attenuation can be accurately calculated will increase.

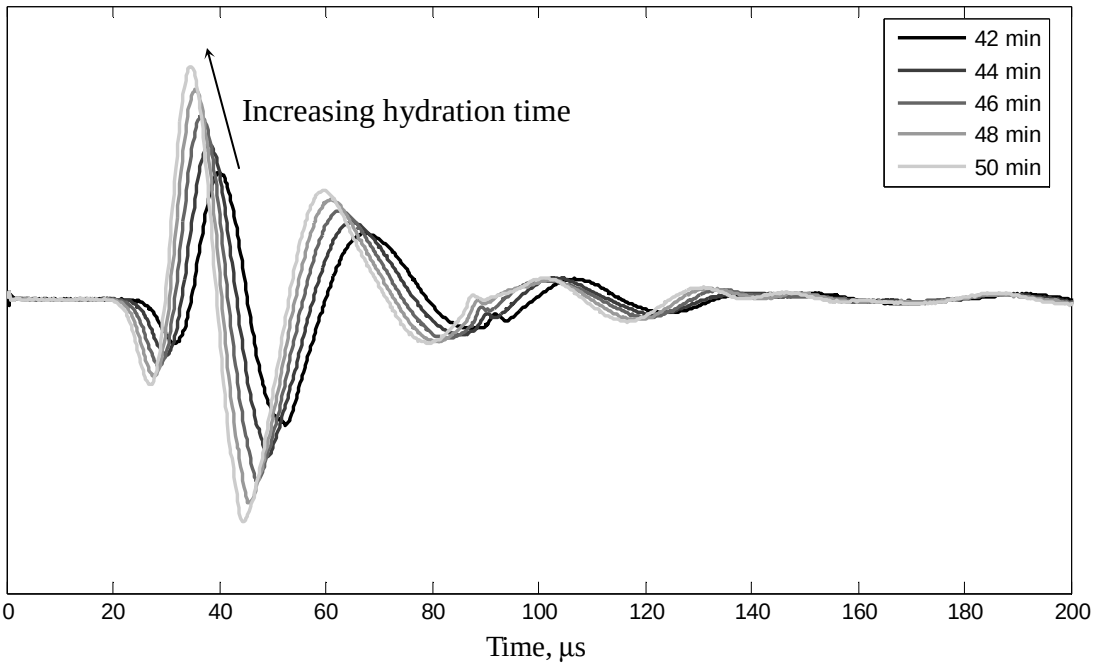

Figure 5.6: Wave development with hydration time in the time domain for CP05

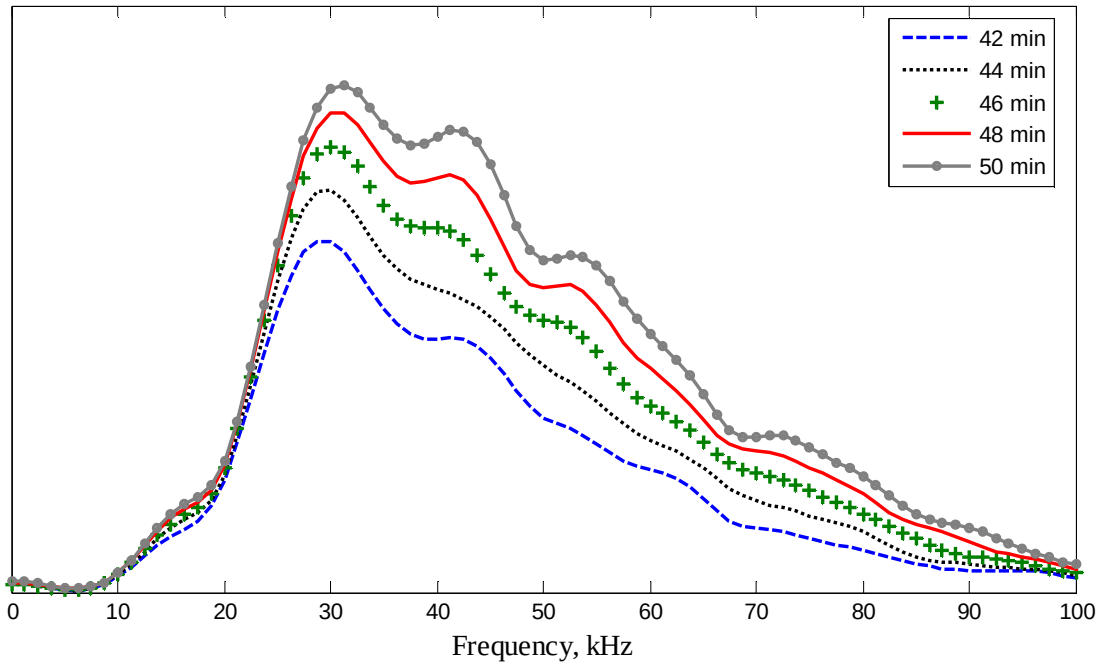

Figure 5.7: Wave development with hydration time in the frequency domain for CP05

In addition to monitoring the wave development as a function of time, the phase velocity and attenuation were calculated at 40, 45, and 50 minutes for CP07 as seen in Figure 5.8. In this figure, it is seen that the phase velocity increases and the attenuation decreases with time. As mentioned previously, the fresh cement paste gains strength and stiffness as new hydrates are formed, consequently providing a more rigid medium through which the ultrasonic signals travel. Additionally, considering the hydration products occupy twice the volume of the originals solids—the cement—at 100% hydration, the solid or skeletal fraction of the mix is increasing with hydration. Therefore the increase in phase velocity and decrease in attenuation as a function of time can be explained by an increase in rigidity or transversely an increase in total solids. Because the phase velocity and attenuation are changing fairly significantly with time, it is clear that in order to compare these characteristics across different levels of AEA, measurements must be taken at nearly identical hydration times.

5.1.3 Variation in Ultrasonic Signals as a Function of level of AEA

A final set of ultrasonic tests was performed in order to calculate and compare ultrasonic phase velocity and attenuation for cement pastes with increasing levels of AEA. As mentioned in Chapter 4, phase velocity and attenuation are calculated by comparing two measurements in the same paste at two distinct separation distances taken 20 seconds apart. This data was recorded at a hydration time of 40 minutes for two replicate cement paste samples for each of the five levels of AEA: 0% (CP01, CP02), 0.1% (CP03, CP04), 0.2% (CP05, CP06), 0.4% (CP07, CP08), 0.8% (CP09, CP10). Because the two different

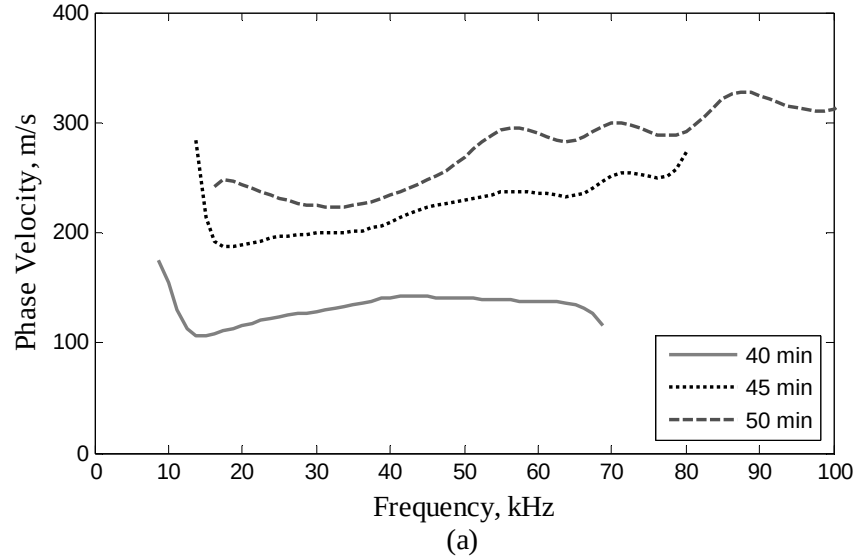

(a)

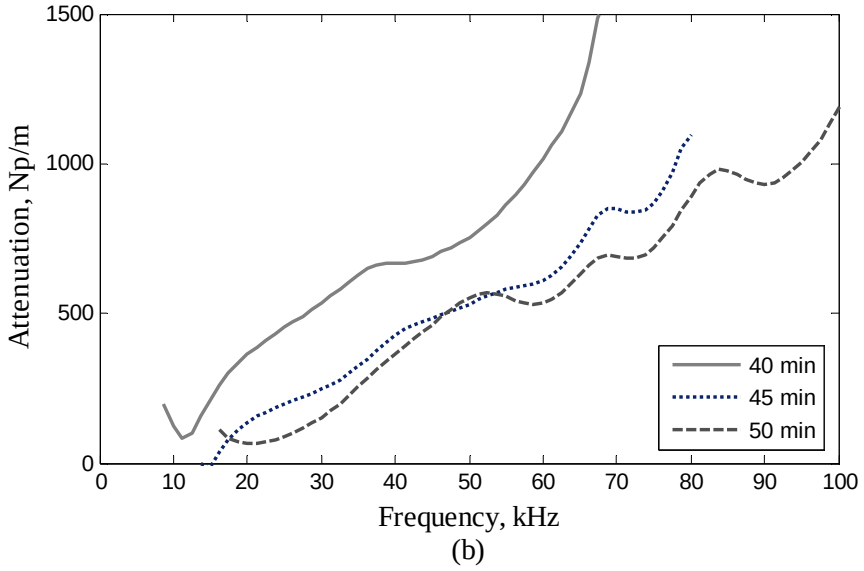

(b)

Figure 5.8: Phase velocity and attenuation with hydration time

waves in the 0.35 w/c non-air entrained pastes are difficult to separate from each other, it is difficult to systematically window the second, slower wave for the purpose of calculating phase velocity and attenuation. Therefore, the phase velocity and attenuation for the slow wave in the non-air entrained mixes are less consistent and predictable. The mean phase velocities for each of the five levels of AEA are shown in Figure 5.9. Each phase velocity is only plotted for the valid frequency range where the frequency spectrum showed sufficient signal amplitude to provide reasonable results. In some of the test sets for a given level of AEA, the two phase velocities are very close to one another as seen in Figure 5.10. However not all test sets showed such low variance, as for the 0.8% AEA mixes shown in Figure 5.11. For the frequency range of the signals resulting at this point in hydration, the calculated phase velocities do not show a clear trend with level of chemical air entrainer.

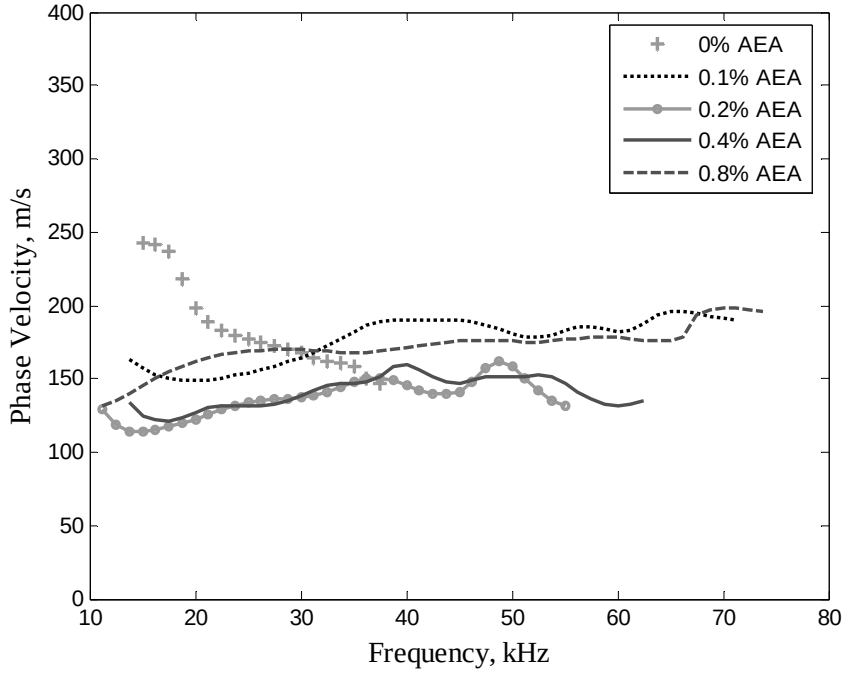

Figure 5.9: Mean phase velocities for varying levels of AEA

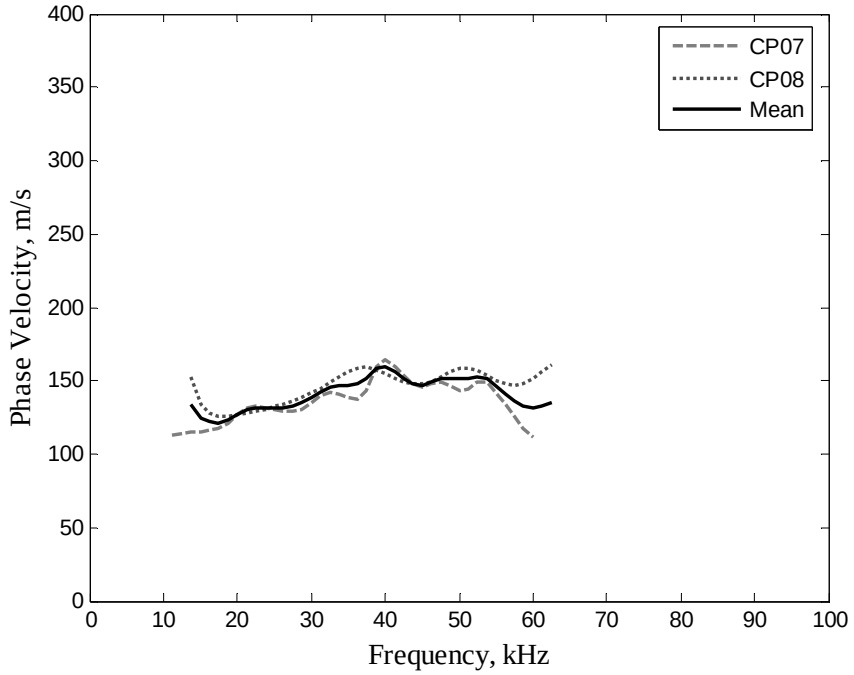

Figure 5.10: Phase velocity for 0.4% AEA

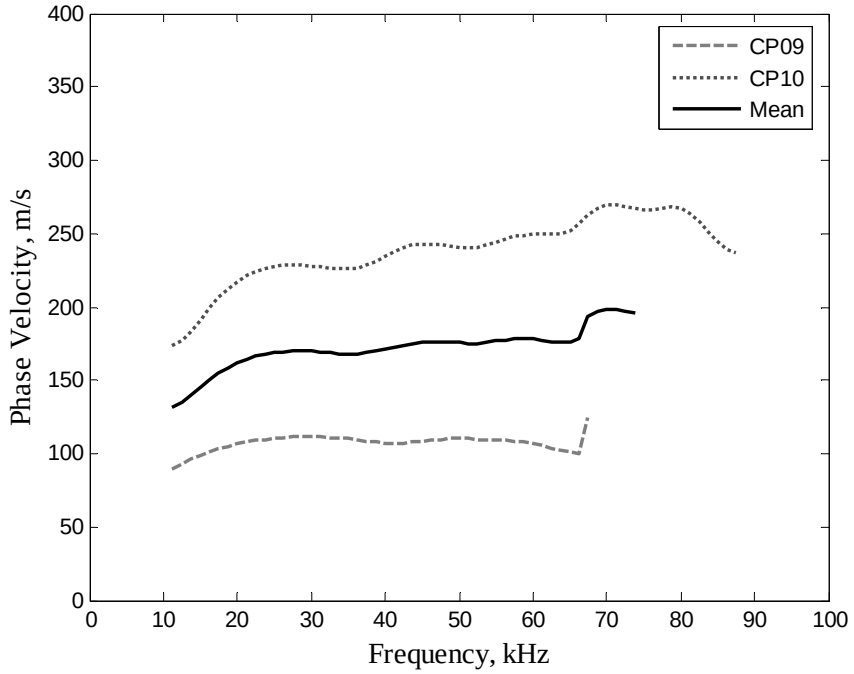

Figure 5.11: Phase velocity for 0.8% AEA

The mean attenuations for each of the five levels of AEA are plotted in Figure 5.12. Again, the attenuations are only plotted for the frequencies which showed sufficient signal strength in the frequency spectrum. Figure 5.13 and 5.14 show the two data sets and the means for the 0.4% and 0.8% AEA mixes respectively. As for the phase velocities, the mean attenuations do not appear to follow a clear trend with increasing levels of AEA.

It is interesting to note that for the 0.8% AEA mixes, the two calculated attenuations have similar slopes, however, the attenuation for CP09 seems to be offset from that of CP10 by almost 600 Np/m. Recall that the void distribution for CP10, as examined by petrographic analysis, was found to be non-uniform, with an increase in air content from 2.1% to 6.2% across the difference halves of the surface. It is possible that the sample of

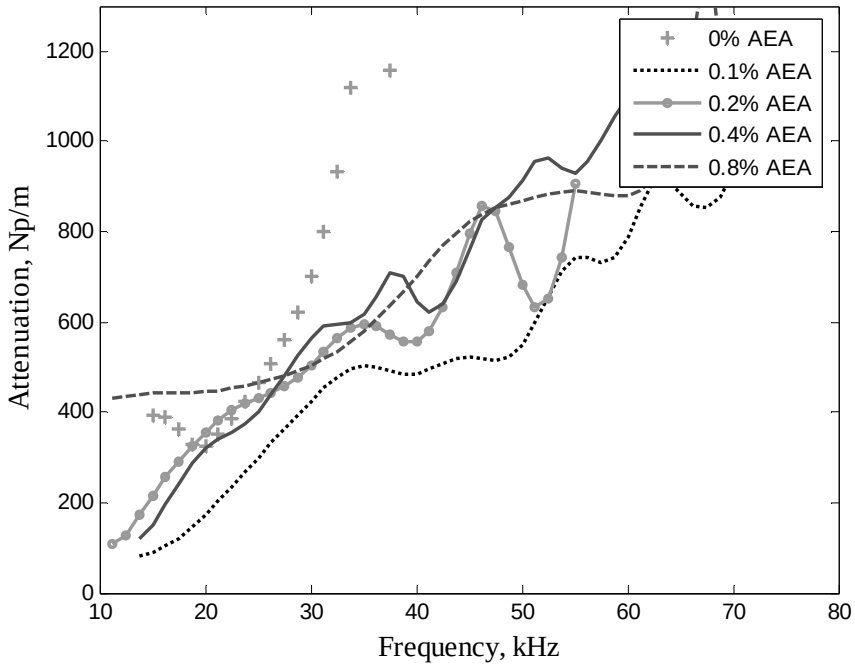

Figure 5.12: Mean attenuations for varying levels of AEA

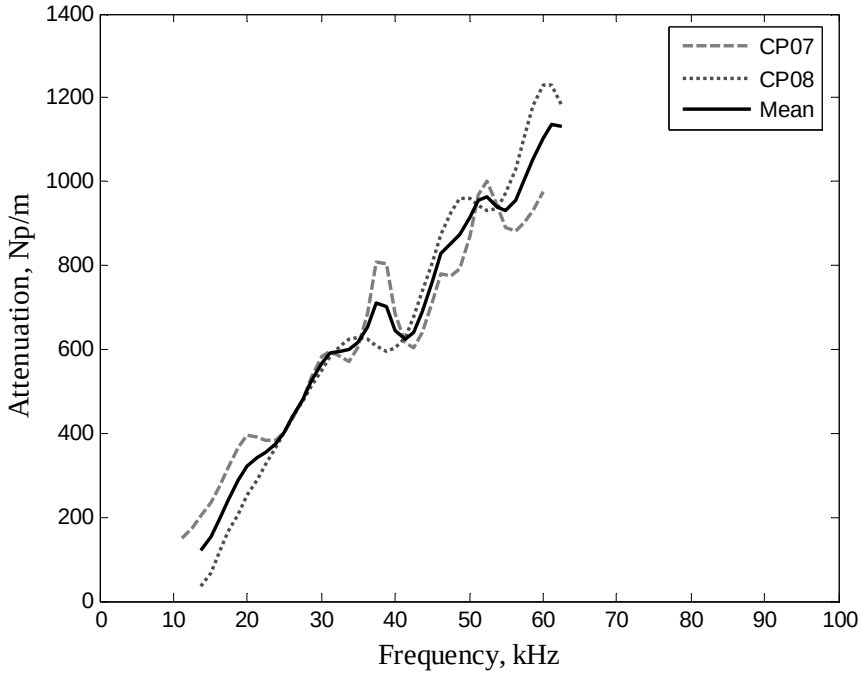

Figure 5.13: Attenuation for 0.4% AEA

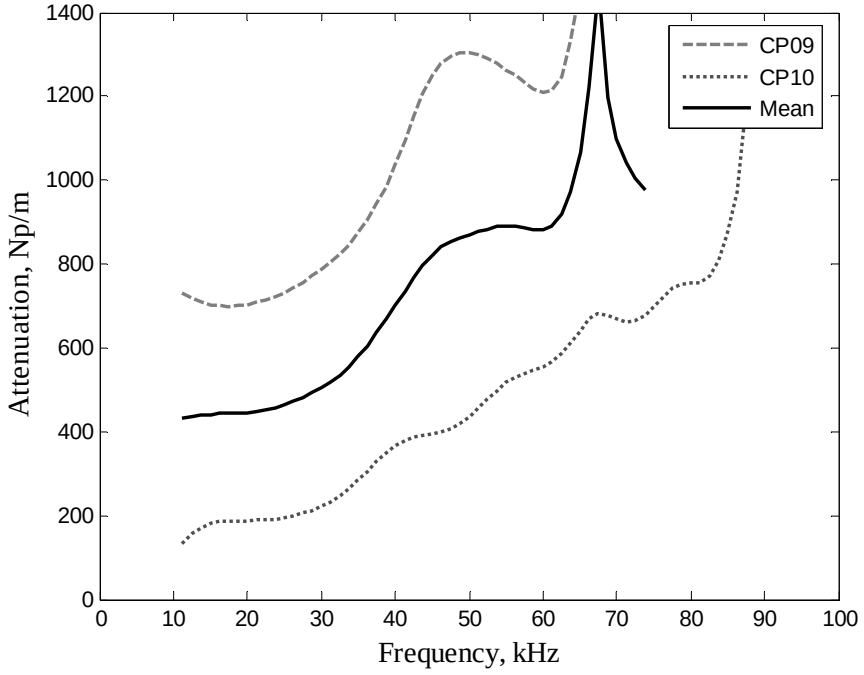

Figure 5.14: Attenuation for 0.8% AEA

paste observed in the ultrasonic testing of CP10 exhibited a significantly lower volume of voids than CP09, which would explain the increased phase velocity and decreased attenuation of CP10. If based on the petrographic results, it is assumed that the air entrainment for CP10 is unreliable, only the phase velocity and attenuation for CP09, not the mean of CP09 and CP10, should be considered for comparison with the other design mixes. As shown in Figures 5.15 and 5.16, a trend is more apparent in the ultrasonic phase velocities and attenuations when the data for CP10 is thrown out. While the calculated phase velocities and attenuations for the 0.2% and 0.4% AEA sample means are very similar, there is an obvious change across the range of air entrainer dosages from 0.1% up to 0.8% AEA. Overall for the modified results which exclude the data from CP10, the phase velocity decreases and the attenuation increases with an increasing level of AEA.

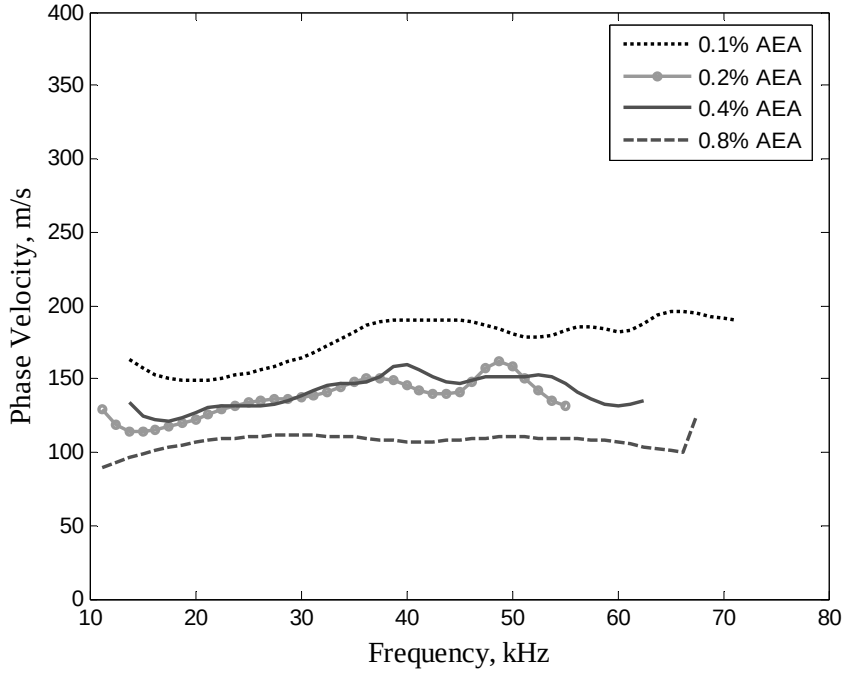

Figure 5.15: Phase velocities for varying levels of AEA, excluding data from CP10

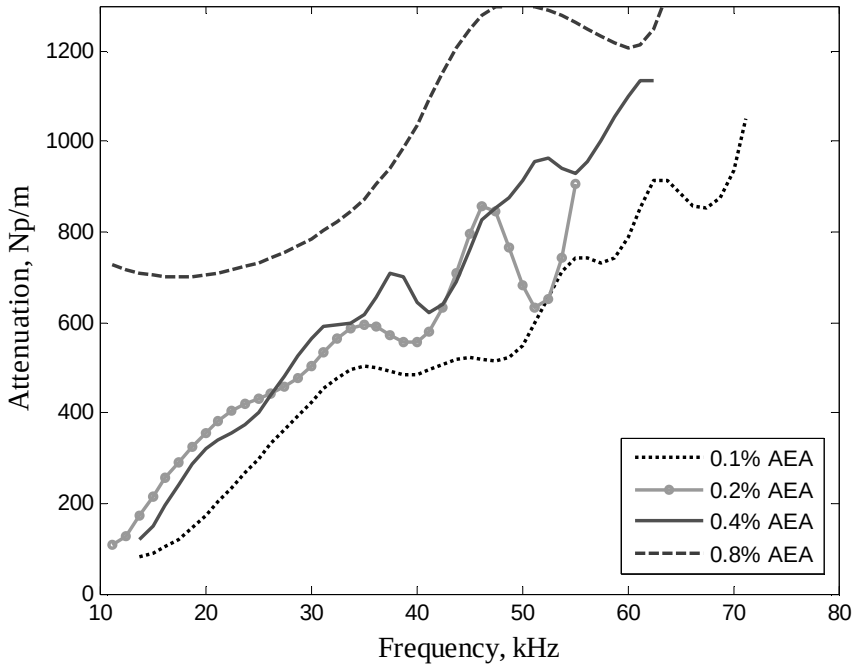

Figure 5.16: Attenuations for varying levels of AEA, excluding data from CP10

In order to discover potential sources of error to further explain the inconsistencies in calculated phase velocity and attenuation, an apparent velocity of the signals with time was compared. The apparent velocity is related to the propagation distance and the arrival time of a given feature of the wave. A true pulse velocity would use the initial disturbance of the wave measured by the transducers as the feature to monitor. However, this initial disturbance is not an ideal feature to monitor in this case, as it is extremely difficult to accurately distinguish this feature for early signals. Instead, the largest trough, or the signal minimum, was chosen as the feature to study and base the apparent velocity. Figure 5.17 shows two signals, one at 24 minutes and one at 40 minutes, and the location representing the arrival time of the monitored feature. The apparent velocity was then calculated to be the transducer separation distance divided by the arrival time.

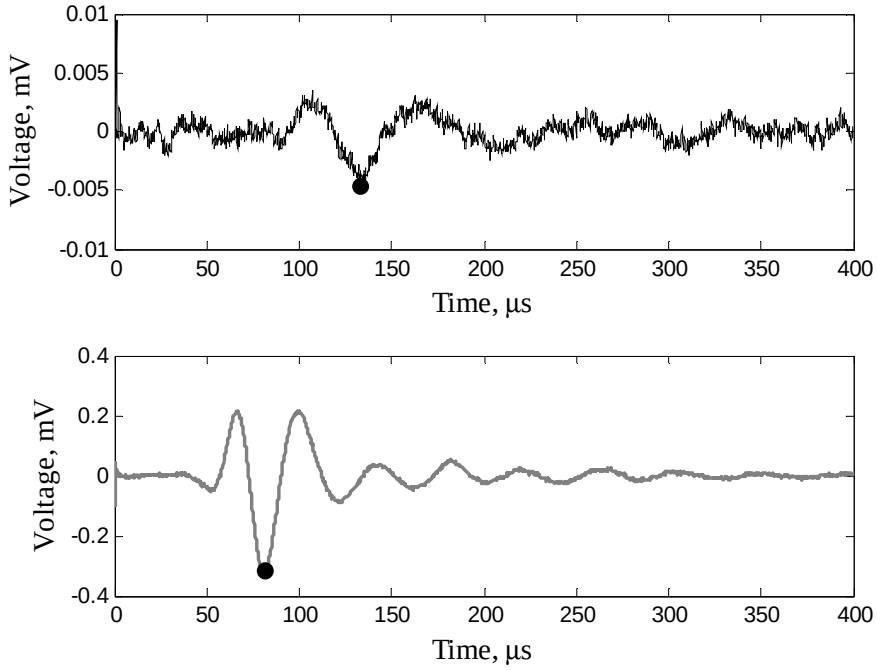

Figure 5.17: Arrival time of signal minimum at 24 minutes (top) and 40 minutes (bottom)

Figure 5.18 shows the apparent velocity with hydration time. Disturbances can be clearly identified in the generally increasing apparent velocities. The circles plotted on each of the curves represent the point in time when the transducers were moved. It should be noted that, in general, the apparent velocity drops when the transducers are moved, especially past the first 35 minutes of hydration as the paste stiffness increases. Following the drop, the apparent velocity undergoes a period of more rapid increase, leveling out to a slope similar to that before the disturbance. While initial set does not occur until after 2 hours and the paste is therefore still in plastic form, it is clear that the movement of the transducers does disturb either the coupling between the transducers and the paste, or the properties of the bulk paste between the transducers. It is possible that this disturbance is only temporary, however, under the current measurement procedure,

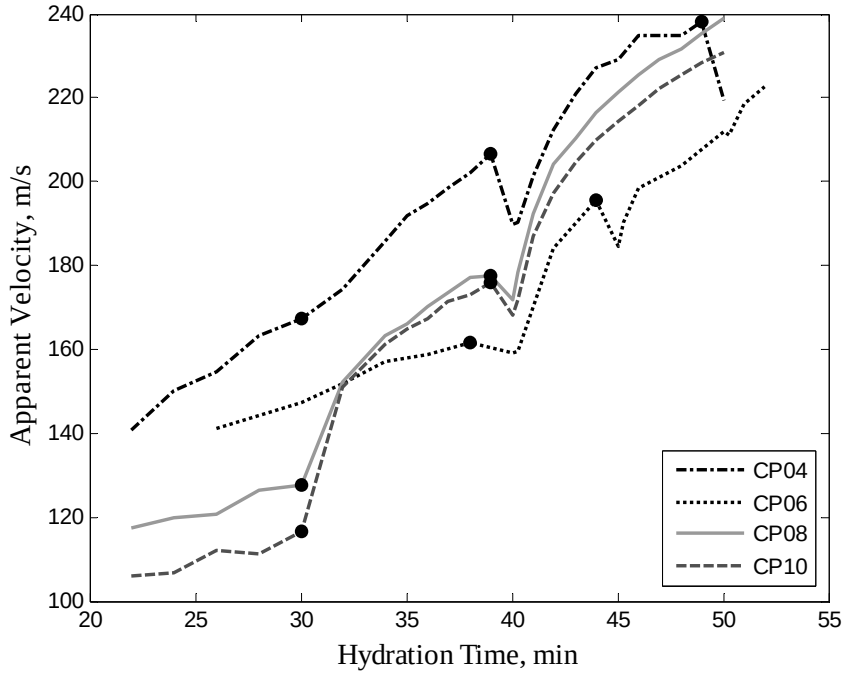

Figure 5.18: Apparent velocity with hydration time

phase velocity and attenuation are calculated by comparing two signals that are acquired subsequent to transducer movement. Therefore, this disturbance critically disrupts the resulting phase velocities and attenuations, and increases their inaccuracies and inconsistencies. However, the exact magnitude of these discrepancies is unknown.

The true solution to circumvent the issues due to paste disturbance around the transducers is to maintain constant transducer separation. To measure two ultrasonic signals with different propagation distances without relying on the reflected signal, an apparatus using three transducers—one large source transducer but two receiving transducers at different distances from the source—could be used. Additional improvement is possible if the signals can be compared for higher frequencies. This would improve the device's

sensitivity to the smaller, entrained air voids. Because the transducers are stationary in the single source-two receivers setup, phase velocity and attenuation could be monitored up to or even past initial set of the paste. As seen in Figure 5.7, this would increase the signal energy at higher frequencies and therefore increase the frequencies for which phase velocity and attenuation could be calculated. However, further investigation would be needed to ensure that the highly basic cement paste would not damage the transducers. A third improvement made possible by the single source two transducers device is that it removes the 20 second time difference between compared signals and allows for continuous monitoring of phase velocity and attenuation in real time.

CHAPTER 6

CONCLUSION AND OUTLOOK

Because of the existence of the fast and slow waves unique to non-air entrained samples, ultrasonic measurements can clearly distinguish between air entrained and non-air entrained cement paste. Therefore based on the raw ultrasonic waveform, it can be immediately determined whether or not chemical air entrained was in fact included in the mix. Additionally, the two-wave phenomenon in non-air entrained fresh cement paste follows the model described by Biot in his theory for wave propagation in a fluid-saturated porous media, which predicts the existence of a fast and slow pressure wave [27-30]. Because the characteristics of the first, or fast wave appear to mimic those of water, it is believed that one of the material phases and/or propagation modes is dominated by water channels or paths.

Previous work has shown ultrasonic attenuation can measure air content and detect a difference between entrained and entrapped air in hardened cement paste specimens [4]. However ultrasonic phase velocity and attenuation measurements made with the proposed procedure and its resulting frequency range cannot distinguish between varying air contents with sufficient accuracy to enable a quantitative inversion procedure. It is believed that the current device is limited by the relatively low frequency range of the received signal. Furthermore, disruption of the plastic cement paste and its coupling with the transducers due to transducer movement contributes to inaccuracies in the data. Based on the petrographic analysis, it is also possible that part of the inconsistency in

phase velocity and attenuation may be due to inconsistencies in the air entrainer effectiveness or void distribution leading to variations in the resulting air void system.

Future work should develop a new model of the immersion device that utilizes a single source with two receiving transducers at different distances from the source in order to remove the necessity to more the transducers. The single source ensures that the generated impulse is identical for both propagation paths, reducing discrepancies in the source signal that would inevitably be present if four transducers—two transmitters and two receivers—were used instead of three. However a four transducers setup would still be preferable to the two transducer setup used for this research because it still eliminates the necessity of moving the transducers. This device has the potential to monitor the paste hours into hydration, which could provide an increased frequency range for the phase velocity and attenuation data. It also would provide for continuous attenuation monitoring through time, increasing the amount of data for each sample and therefore increasing the reliability of the results. Future work could also study the possibility of using an ultrasonic immersion device to monitor strength and stiffness development. An ultrasonic test to determine initial and final set in situ could be developed and would be very valuable to the construction industry.

APPENDIX A

ADDITIONAL ULTRASONIC DATA

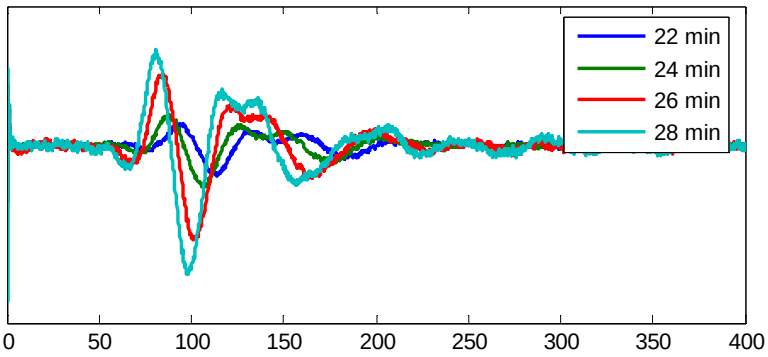

(a)

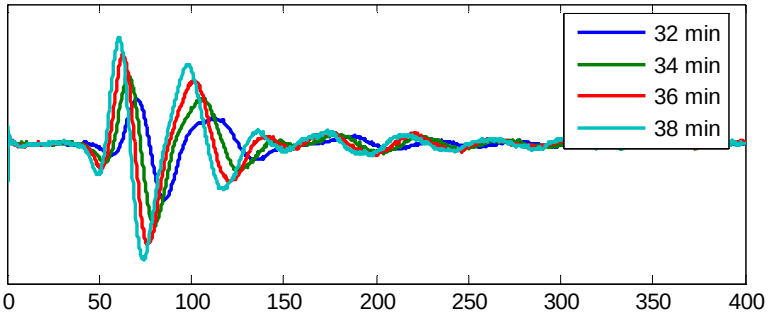

(b)

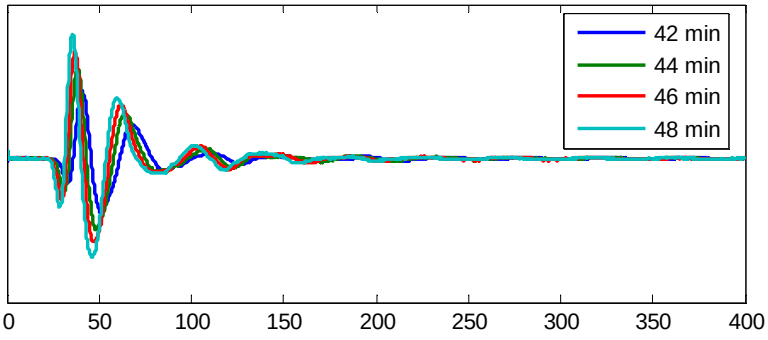

(c)

Figure A.1: Wave development with hydration time in the time domain for CP03

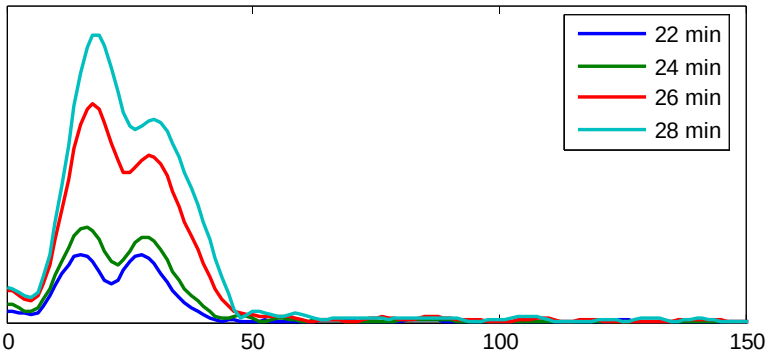

(a)

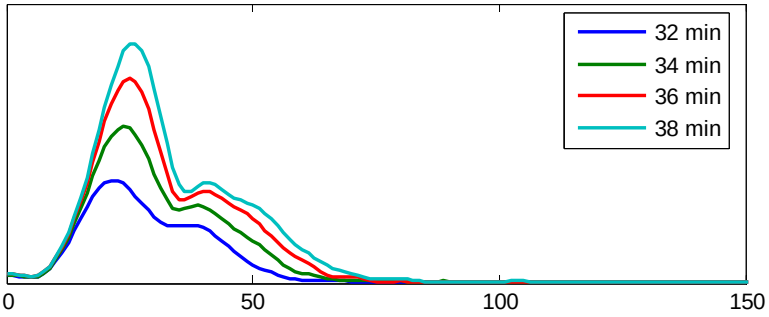

(b)

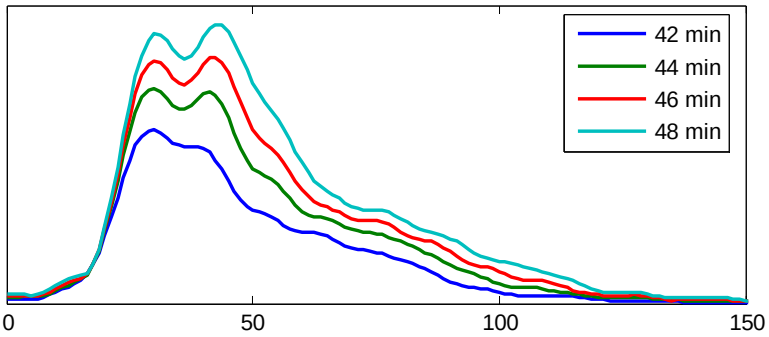

(c)

Figure A.2: Wave development with hydration time in the frequency domain for CP03

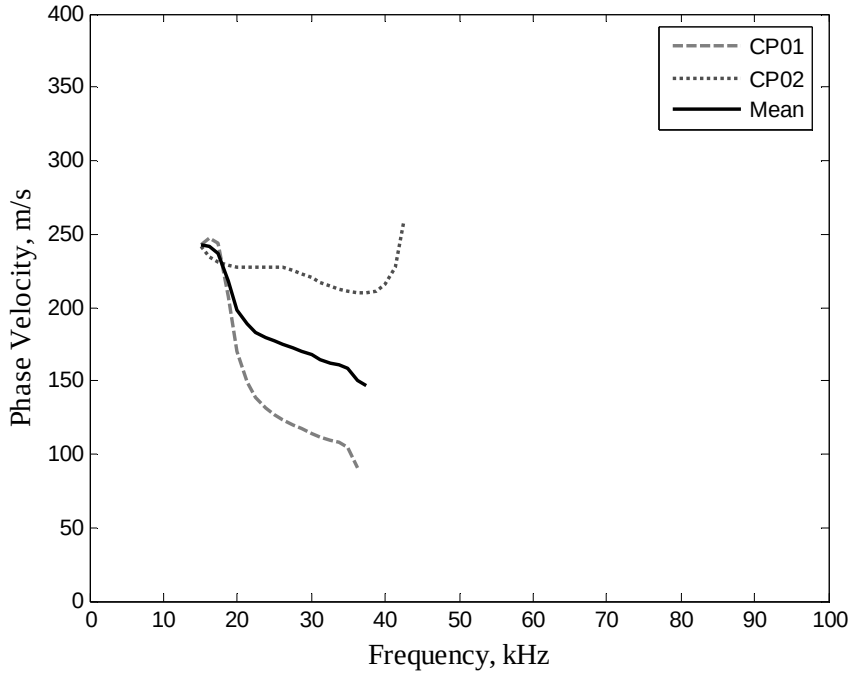

Figure A.3: Phase velocity for 0% AEA or non-air entrained

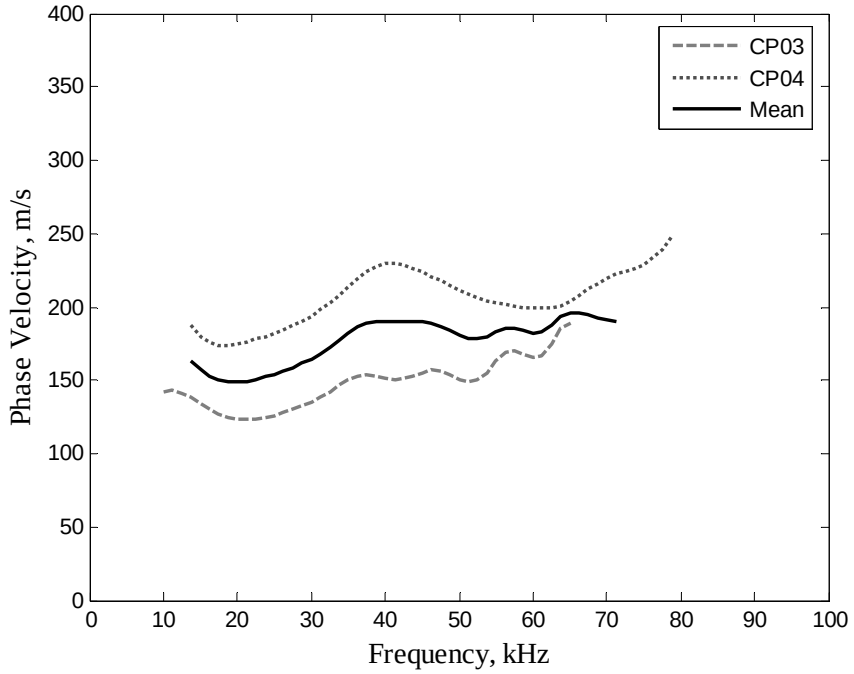

Figure A.4: Phase velocity for 0.1% AEA

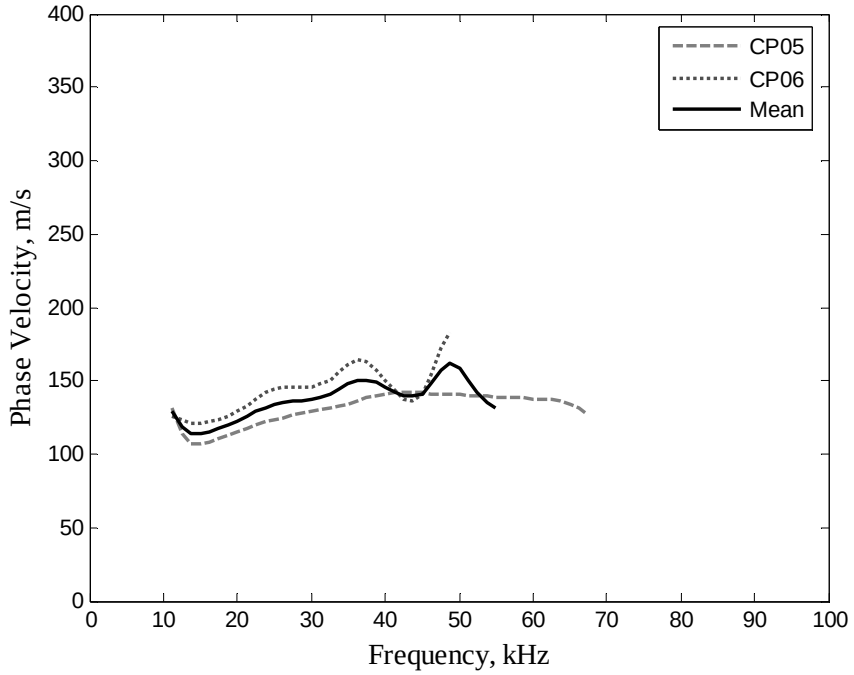

Figure A.5: Phase velocity for 0.2% AEA

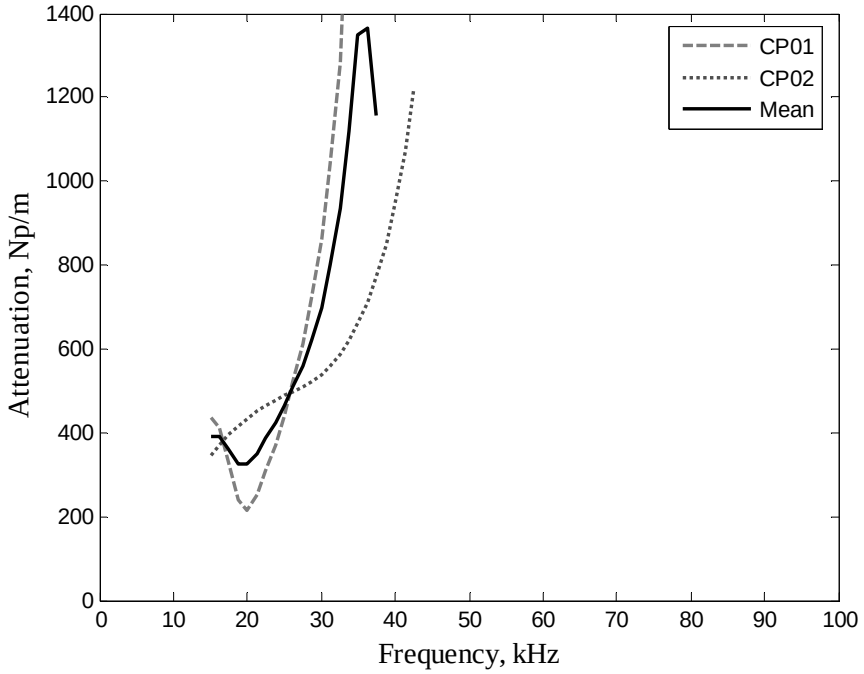

Figure A.6: Attenuation for 0% AEA or non-air entrained

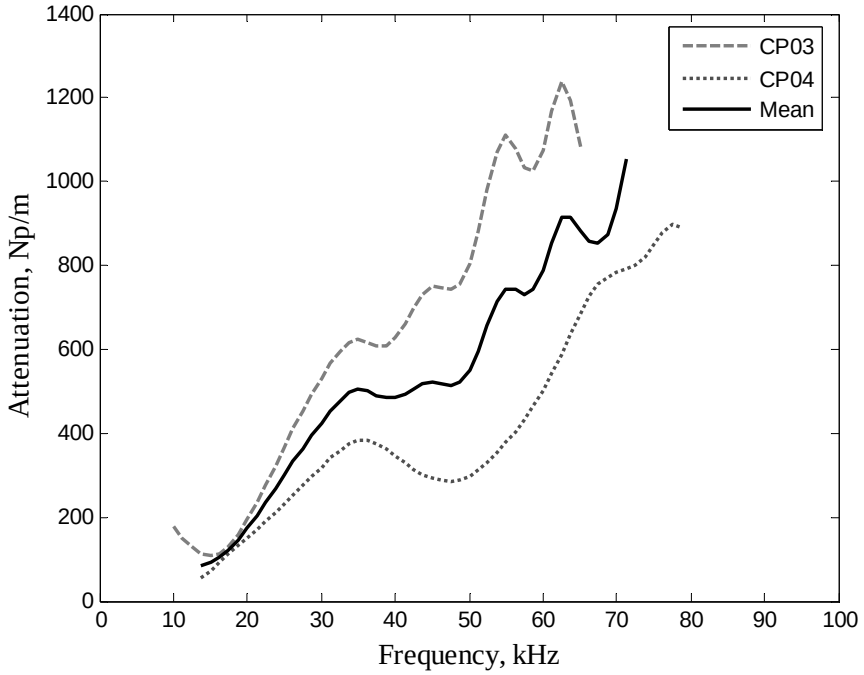

Figure A.7: Attenuation for 0.1% AEA

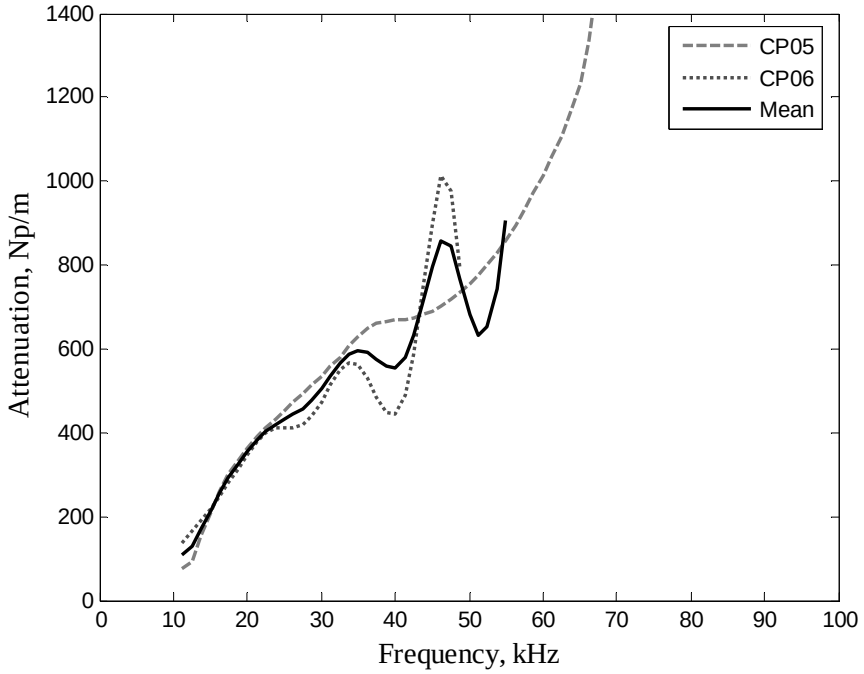

Figure A.8: Attenuation for 0.2% AEA

REFERENCES

[1] ASTM Standard C 231-08c - Standard Test Method for Air Content of Freshly Mixed Concrete by the Pressure Method *American Society of Testing and Materials.* West Conshohocken, PA, 2008.

[2] ASTM Standard C 173-08a - Standard Test Method for Air Content of Freshly Mixed Concrete by the Volumetric Method. *American Society of Testing and Materials.* ASTM International, West Conshohocken, PA, 2008.

[3] ASTM Standard C 138-08 - Standard Test Method for Density (Unit Weight), Yield, and Air Content (Gravimetric) of Concrete. *American Society of Testing and Materials.* West Conshohocken, PA, 2008.

[4] Punurai, W. "Cement Based Materials' Characterization using Ultrasonic Attenuation." Georgia Institute of Technology, Atlanta, GA, 2006.

[5] Punurai, W., Jarzynski, J.,Qu, J., Kim, J.-Y., Jacobs, L.J. and Kurtis, K. "Characterization of multi-scale porosite in cement paste by advanced ultrasonic techniques." *Cement and Concrete Research.* 37:38–46, 2007.

[6] Punurai, W., Jarzynski, J.,Qu, Kurtis, K. and Jacobs L.J. "Characterization of entrained air voids in cement paste with scattered ultrasound." *NDT&E International.* 39:514-524, 2006.

[7] Reinhardt, H. W., Grosse, C. U., and Herb, A. T. "Ultrasonic monitoring of setting and hardening of cement mortar—a new device." *Materials and Structures*, 33:580-583, 2000.

[8] Sayers, C. M. and Dahlin, A. "Propagation of Ultrasound Through Hydrating Cement Pastes at Early Times." *Advanced Cement Based Materials*, 1:12-21, 1993.

[9] Oztuk, T., Kroggel, O., Grubl, P., and Popovics, J. S. "Improved ultrasonic wave reflection technique to monitor setting of cement-based materials." *NDT&E International*, 39:258-263, 2006.

[10] Sayers, C. M., and Grenfell, R. L., "Ultrasonic propagation through hydrating cements." *Ultrasonics*, 31:147-153, 1993.

[11] Kmack, Richard. “Characterization of Air Voids in Fresh Cement Paste through Ultrasonic Nondestructive Testing.” Georgia Institute of Technology, Atlanta, GA, 2008.

[12] Mehta, P. K. and Monteiro, P. J. M. *Concrete: Microstructure, Properties, and Materials (1st edition)*. New York: McGraw Hill, 1993.

[13] Young, J. F., Mindess, S., Gray, R. J., and Bentur, A. *The Science and Technology of Civil Engineering Materials*. Upper Saddle River: Prentice Hall, 1998.

[14] Kosmatka, S., Kerkhoff, B., and Panarese, W., *Design and Control of Concrete Mixtures, 14th Edition*, Skokie: Portland Cement Association, 2009.

[15] ASTM Standard C 33/C 33M-87 - Standard Specification for Concrete Aggregates. *American Society of Testing and Materials.* West Conshohocken, PA, 2008.

[16] Dodson, V. H. *Concrete Admixtures*. New York: Van Nostrand Reinhold, 1990.

[17] Du, L. and Folliard, K. J. “Mechanisms of air entrainment in concrete.” *Cement and Concrete Research.* 35:1463-1471, 2005.

[18] Edmeades, R. M. and Hewlett, P. C. “Cement Admixtures.” *Lea’s Chemistry of Cement and Concrete (fourth edition).* Ed. Peter C. Hewlett. London: Arnold, 1998.

[19] ACI Committee 201 – Guide for making a condition survey of concrete in service (ACI 201.R-92). American Concrete Institute. Famington Hills, Mich., 1992

[20] ASTM Standard C 457-08d - Microscopical Determination of Parameters of the Air-Void System in the Hardened Concrete. *American Society of Testing and Materials.* West Conshohocken, PA, 2008.

[21] Grove, J., Steffes, B., and Anderson-Wilk, M. “Using the Air Void Analyzer for Real-Time Quality Control Adjustment in the Field.” National Concrete Pavement Technology Center, Iowa State University. May 2006.

[22] Achenbach, J. D. *Wave propagation in elastic solids*. New York: Elsevier, 1975.

[23] Kinsler, L. E., Frey, A. R., Coppens, A. B., and Sanders, J. V. *Fundamentals of Acoustics (third edition)*. New York: John Wiley & Sons, 1982.

[24] Papadakis, E. P. “Ultrasound attenuation caused by scattering in polycrystalline metals.” *Journal of the Acoustical Society of America*, 37:711-717, 1965.

[25] Lévêque, G., Rosenkrantz, E., and Laux, D. “Correction of diffraction effects in sound velocity and absorption measurements.” *Measurement Science and Technology.* 18:3458-3462, 2007.

[26] Rogers, P. H. and Van Buren, A. L., “An exact expression for the Lommel diffraction correction integral.” *Journal of the Acoustical Society of America.* 55:724-728, 1974.

[27] Biot, M. A. “Generalized Theory of Acoustic Propagation in Porous Dissipative Media.” *Journal of the Acoustical Society of America.* 34:1254-1264, 1962.

[28] Biot, M. A. “Theory of Propagation of Elastic Waves in a Fluid-Saturated Porous Solid, 1. Low-Frequency Range.” *Journal of the Acoustical Society of America.* 28:168-178, 1956.

[29] Bourbié, T., Coussy, O., and Zinszner, B. *Acoustics of Porous Media*. Houston: Gulf Publishing Company, 1987.

[30] Chotiros, N. P. “Biot Model of Sound-Propagation in Water-Saturated Sand.” *Journal of the Acoustical Society of America.* 97:199-214, 1995.

[31] Aggelis, D.G. and Philippidis, T.P. “Ultrasonic wave dispersion and attenuation in fresh mortar.” *NDT&E International* 37:617–631, 2004.

[32] ASTM Standard C 150-07 - Standard Specification for Portland Cement. *American Society of Testing and Materials.* West Conshohocken, PA, 2007.

[33] ASTM Standard C 114-09 - Standard Test Methods for Chemical Analysis of Hydraulic Cements. *American Society of Testing and Materials*. West Conshohocken, PA, 2009.